Proposal

P-877

Measurement of the Magnetically-Induced QED Birefringence of theVacuum and An Improved Laboratory Search for Light Pseudoscalars

Siu Au Lee, William M. Fairbank, Jr. and Walter H. Toki

Department of Physics, Colorado State University
Fort Collins, Colorado 80523

John L. Hall

Joint Institute for Laboratory Astrophysics
University of Colorado and The National Institute of Standards and Technology
Boulder, Colorado 80309

Patrick Colestock, Vernon Cupps, Hans Kautzky, Moyses Kuchnir,
Frank Nezrick and Robert Noble

Fermi National Accelerator Laboratory
Batavia, Illinois 60510

Submitted to
Fermi National Accelerator Laboratory

November 16, 1998

Co-spokespersons:

Siu Au Lee
Phone:(303) 491-6389
FAX: (303) 491-7947
Email: salee@lamar.colostate.edu

Frank Nezrick
Phone: (630) 840-4604
FAX: (630) 840-4552
Email: nezrick@fnal.gov

TABLE OF CONTENTS

1. INTRODUCTION

This collaboration, consisting of Colorado State University, University of Colorado and NIST at Boulder, and Fermilab, has studied the feasibility of a high sensitivity QED birefringence measurement and laboratory search for light pseudoscalars. We propose to measure, for the first time, the birefringence induced in the vacuum on a light beam travelling in a powerful magnetic field. The same experimental setup also allows a highly sensitive search for light pseudoscalar particles. The experiment will combine custom-designed optical heterodyne interferometry with a string of two SSC prototype superconducting dipole magnets operated at the E-4R site of Fermilab. With these powerful laser tools, sensitivity advances of 10^6 to 10^8 over previous optical experiments will be possible. The proposed experiment will be able to measure the QED light-by-light scattering effect with a 0.5 % precision. The increased sensitivity for the pseudoscalar to two photon interaction will result in a bound on this process rivalling the results based on astrophysical arguments. In addition, the laser measurement techniques developed for this experiment will have impact on the next generation of accelerator technology and optical metrology.

In this proposal we address the scientific significance of the experiment, and propose a new birefringence measurement scheme. We examine systematic effects which may degrade the measurement sensitivity, and propose techniques to overcome these problems. Notable challenges arise in the area of seismic vibration isolation, reduction of background gas contamination and mirror heating effects. The experimental scheme is designed to provide a sensitivity in measuring the change in the index of refraction at the 7×10^{-25} level, a domain which the gravitational wave detector groups regard as probable but not guaranteed. The fundamental advantage of our technique is that it utilizes differential measurements in several aspects, thus elegantly suppressing unwanted noises.

It has been three years since this proposal was initially submitted. During that period our collaboration has made significant progress in developing the laser and vibration isolation systems, and locking techniques. A rudimentary experimental area has been developed at E-4R which contains the SSC dipole magnet system, laser systems and initial prototypes of the seismic vibration isolation systems for supporting the interferometer mirrors. At CSU, a two meter Fabry

Perot interferometer is under development, and a laser stabilized by locking to a Doppler suppressed hyperfine line of I_2, with a linewidth below 10 Hz, is in operation. At JILA, a dual mode cavity locking technique is being developed, and the polarization memory of the diclectric mirrors is being investigated. Several graduate students are already dedicated to these developments.

We present a five year experimental program divided into a three year Phase I and a two year Phase II. In Phase I, the two meter Fabry Perot Interferometer is used as a test-bed for developing simple and dual mode locking techniques, and the 50 m Fabry Perot Interferometer is constructed and demonstrated to achieve a sensitivity at the QED level. During Phase I the questions to be addressed include: investigation of laser power effects on the birefringence of mirrors, development of anti-seismic passive and active suspension systems and mirror control systems, demonstration of laser locking of sufficient range and accuracy, development of the laser beam-steering and mirror automatic alignment system, and investigation of the light scattering problem and photodesorption in the beam tube. In Phase II the magnet system is commissioned. Viable magnet ramp rates are confirmed and beam tube getter system is developed. In year 4, full integration of the optical and magnet systems occurs. The 50 m interferometer will be used for initial measurements. In the final year a precision measurement of the QED effect will be performed and in the process a search for light pseudoscalars will be conducted.

2. REVIEW OF THEORY AND SIGNIFICANCE OF THE EXPERIMENT

2.1 Magnetic Birefringence and Dichroism in Vacuum

When a beam of light travels in vacuum in a strong external magnetic field, the vacuum polarization process of QED induces a small change in the index of refraction of the vacuum. This effect may be interpreted as light-by-light scattering between an optical photon of frequency ω and a zero frequency photon from the magnetic field (Fig. 2.1). For a light beam traveling in a direction perpendicular to the applied field **B** and linearly polarized at 45° to **B**, this QED effect leads to a slower travel speed for the polarization component parallel to **B** than for that perpendicular to **B**, resulting in a small elliptical polarization in the light beam. The vacuum, in effect, becomes birefringent, i.e., it has a different index of refraction for the two polarizations. A polarized light beam in a magnetic field may also interact with scalar or pseudoscalar bosons such as the axion to produce a birefringence as well as a rotation, or dichroism, of the polarization. Thus a precision measurement of the optical birefringence and optical rotation of a laser beam in a strong magnetic field can be used to test QED, and to search for scalar or pseudo-scalar particles.

2.2 QED Birefringence

2.2.1 Theory of the Dominant Magnetic Birefringence Diagram in QED

Nearly sixty years ago, Euler and Heisenberg [1] derived an effective Lagrangian for a constant electromagnetic field in vacuum which included corrections due to vacuum polarization (Fig. 2.1a). This Lagragian may be written as

$$L_{eff} = \left(\frac{1}{8\pi}\right)(E^2 - B^2) + \left(\frac{2\alpha^2}{45(4\pi)^2 m_e^4}\right)\left[(E^2 - B^2)^2 + 7(E\cdot B)^2\right] \qquad (2.1)$$

(Natural Lorentz-Heavyside units, in which $\hbar = c = 1$ and $\alpha = e^2/4\pi = 1/137$, are used here.) In 1971, Adler derived the result for the magnetically-induced birefringence of the vacuum using the Euler-Heisenberg Lagrangian [2]. The difference in the index of refraction for light beams polarized parallel and perpendicular to the external magnetic field is given by

$$n_{//} - n_{\perp} = \left(\frac{\alpha}{30\pi}\right)\left(\frac{B}{B_{cr}}\right)^2 \qquad (2.2)$$

where $B_{cr} = m_e^2/e = 4.41\times10^9$ T is a characteristic field at which the QED effect becomes large. The corresponding ellipticity induced in a laser beam of wavelength λ, linearly polarized at 45° to the magnetic field and making N passes through the field region of length l, is

$$\psi_{QED} = \frac{N(n_{//}-n_{\perp})\pi l}{\lambda} = \frac{Nl}{\lambda}\left(\frac{\alpha}{30}\right)\left(\frac{B}{B_{cr}}\right)^2 \qquad (2.3)$$

Here the ellipticity is defined as half of the phase difference between the two polarization components. It is clear that in order to observe ψ_{QED}, l, N and B should be as large as possible.

For representative values, consider a green laser (λ = 532 nm) propagating in a string of two SSC prototype magnets (B = 6 T, l = 30 m). A high finesse Fabry-Perot cavity will be used to pass the light beam many times ($N = 2.5\times10^4$) through the field region. Eqs. (2.2) and (2.3) give $n_{//} - n_{\perp} = 1.4\times10^{-22}$ and $\psi_{QED} = 6.3\times10^{-10}$ rad. Although these values are very small, the calculated shot noise limited sensitivity in the proposed experiment is 3.4×10^{-9} rad/$\sqrt{\text{Hz}}$, which corresponds to reaching the QED effect in 5 seconds. A 0.5% precision, as proposed in this experiment, will require averaging data for about 56 hours at the shot-noise limited level.

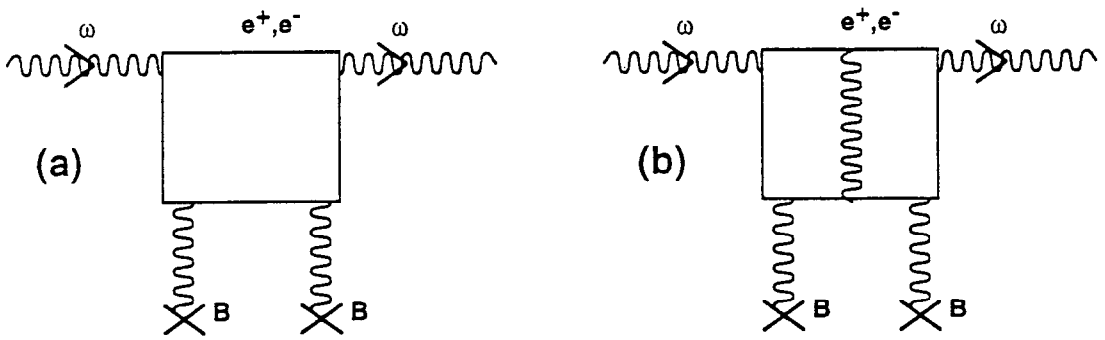

FIG. 2.1 Feynman diagrams for light-by light scattering producing magnetic birefringence in vacuum: (a) The dominant term, of order $(\alpha/\pi)B^2$. (b) One of the second order diagram with radiative correction, of order $(\alpha/\pi)^2B^2$.

2.2.2 Higher Order QED Corrections to Magnetic Birefringence

One of the second order light-by-light scattering diagrams is shown in Fig. 2.1b. Radiative corrections such as Fig. 2.1b are expected to be of order (α/π) compared to the

dominant diagram Fig. 2.1a. The second order correction to the Lagrangian has been derived from the Euler-Heisenberg integral form by Ritus [3]. The result is

$$L_{eff}^{(2)} = \left(\frac{\alpha^3}{\pi (4\pi)^2 m_e^4}\right) \left[\left(\frac{16}{81}\right) (E^2 - B^2)^2 + \left(\frac{263}{162}\right) (E \cdot B)^2\right] \qquad (2.4)$$

Notice that, except for different coefficients, this term has a similar form to the dominant first-order Lagragian. Thus it is straightforward to derive an expression for the index difference to second order:

$$n_{/\!/} - n_{\perp} = \left(\frac{\alpha}{30\pi} + \frac{5\alpha^2}{24\pi^2}\right) \left(\frac{B}{B_{cr}}\right)^2 \qquad (2.5)$$

The second-order correction to Δn is predicted to be 1.45% of the dominant term [3]. Thus, a measurement of the QED birefringence at the 0.5% level will provide a test of these correction terms.

2.3 Significance of a Precision Measurement of QED Birefringence

The proposed experiment will be the first direct measurement of the fundamental light-by-light scattering diagram (Fig. 2.1a). This measurement will provide an excellent reference for other precision tests of QED. These include precision measurements of the electron and muon anomalous magnetic moments a_e and a_μ, in which the light-by-light term is a sixth order correction, and Delbrück scattering of MeV photons off the electric field of a nucleus, which is always mixed with contributions from Rayleigh, nuclear and Thompson scattering. To date these measurements have tested and verified the dominant light-by-light diagram to 0.6% for a_e [4], 4.5% for a_μ [5], and 5% for Delbrück scattering [6]. There has not yet been any measurement with sufficient accuracy to observe the effect of the next order QED corrections to light-by-light scattering such as that of Fig. 2.1b.

A new muon g-2 experiment at Brookhaven [7] offers the possibility of a first deduction of the next order light-by-light diagrams (Fig. 2.1b), which arise as 8th order corrections in that experiment. Of particular interest are possibly observable effects or mass limits for "new physics": gauge bosons, such as W_R, Z', Higgs, and SUSY particles, muon or gauge boson substructure, and excited leptons. The verification of QED light-by-light scattering diagrams to

a comparable level in our proposed experiment provides important experimental backing to the extraction of new physics in the new g-2 experiment.

2.4 Magnetic Birefringence and Rotation due to Photon-axion Mixing

Current theories of elementary particles predict that the spontaneous breaking of a global symmetry is accompanied by the existence of a corresponding Goldstone boson. Axions are light, weakly interacting pseudoscalar bosons which were hypothesized by Peccei and Quinn [8] in order to explain the absence of CP violation in strong interactions. Very low mass axions ($m_a \sim 10^{-6}$-10^{-3} eV) are also considered as candidates for dark matter interactions. For brevity, the word "axion" is used loosely in this proposal to describe all axion-like pseudoscalar particles. These hypothetical weakly interacting scalar or pseudoscalar particles can couple by a two-photon vertex, and their coherent interaction with a polarized beam of photons in a strong external magnetic field can produce a birefringence as well as a rotation of the polarization of the light [9]. Thus a precision measurement of the optical birefringence and rotation of a laser beam in a strong magnetic field can be used to search for such particles.

The dominant Feynman diagrams are shown in Fig. 2.2. The Primakoff production term (Fig. 2.2a) leads to a small absorption in the component of the electric field of light parallel to B. This may be observed experimentally as a small rotation of the plane of polarization of the light beam. The virtual axion production process (Fig. 2b) leads to a greater phase retardation of the light component with polarization parallel to B. This effect induces a small elliptical polarization, and hence a birefringence to the light beam. Both effects may be measured by using light with incident polarization at 45° to the magnetic field.

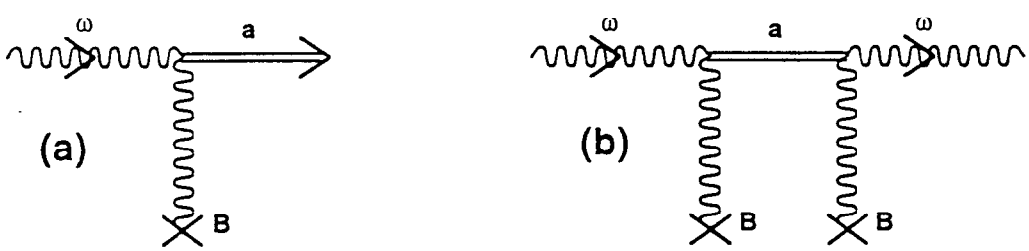

FIG. 2.2 Feynman diagrams for axion-photon coupling leading to (a) magnetic rotation and (b) magnetic birefringence in vacuum.

For a light beam polarized at 45° to the B field, the magnetically induced rotation and ellipticity due to photon and axion-like particle coupling are [9, 10]

$$\epsilon_a = N g_{a\gamma\gamma}^2 B^2 \frac{\omega^2}{m_a^4} \sin^2\left(\frac{m_a^2 l}{4\omega}\right), \qquad (2.6)$$

and

$$\psi_a = \frac{N}{2} g_{a\gamma\gamma}^2 B^2 \frac{\omega^2}{m_a^4} \left[\frac{m_a^2 l}{2\omega} - \sin\left(\frac{m_a^2 l}{2\omega}\right)\right], \qquad (2.7)$$

where $g_{a\gamma\gamma}$ is the axion-photon coupling constant and ω = 2.33 eV is the photon energy. (In the natural Lorentz-Heavyside units, a magnetic field of 1 T can be expressed as 195 eV^2 and a length of 1 m as 5.07×10^6 eV^{-1}.) Both of these effects are linear in N because the axions are not reflected with the photons at the mirrors, but are nonlinear in l because the axion and the photon do not retain exact phase coherence throughout the interaction region since the axion has a mass. Thus it is seen that a longer length l is a substantial advantage at small m_a ($\epsilon_a \propto l^2$ and $\psi_a \propto l^3$). However, much of the advantage is lost for large m_a ($m_a l/2\omega > \pi$) due to the sine functions in Eqs. (2.8) and (2.9). Note that the axion-induced ellipticity ψ_a can be distinguished from the QED induced ellipticity ψ_{QED} through its different dependence upon l.

In the standard Grand Unified Theory (GUT) of elementary particles, the axion mass, m_a, and its coupling constant to two photons, $g_{a\gamma\gamma}$, are related by $m_a(eV)/g_{a\gamma\gamma}(GeV^{-1}) \approx 7.4\times10^9$ and 2.7×10^9, respectively, for DFSZ (leptonic) and KSVZ (hadronic) axions [11]. Although theoretical interest at present centers primarily on axions near the GUT line on a $g_{a\gamma\gamma}$ vs. m_a plot (Fig. 2.3), it is important to investigate experimentally as large a region of the $g_{a\gamma\gamma}$ vs. m_a phase space as possible, since theories do not predict a specific mass for the axion or pseudoscalar particles.

At the present time GUT axions are excluded by laboratory experiments and astrophysical arguments except in two windows, between 2 and 3 eV, and between 10^{-6} and 10^{-3} eV [11]. Above 10^{-3} eV the limits come from particle decay experiments [11], a search for relic axion decay in galactic clusters [13], the duration of the neutrino pulse from SN1987 [14], and arguments based on the lifetime of the sun and the evolution of red giant stars [12]. Possible overclosure of the universe leads to GUT axion exclusion below 10^{-6} eV. [11]

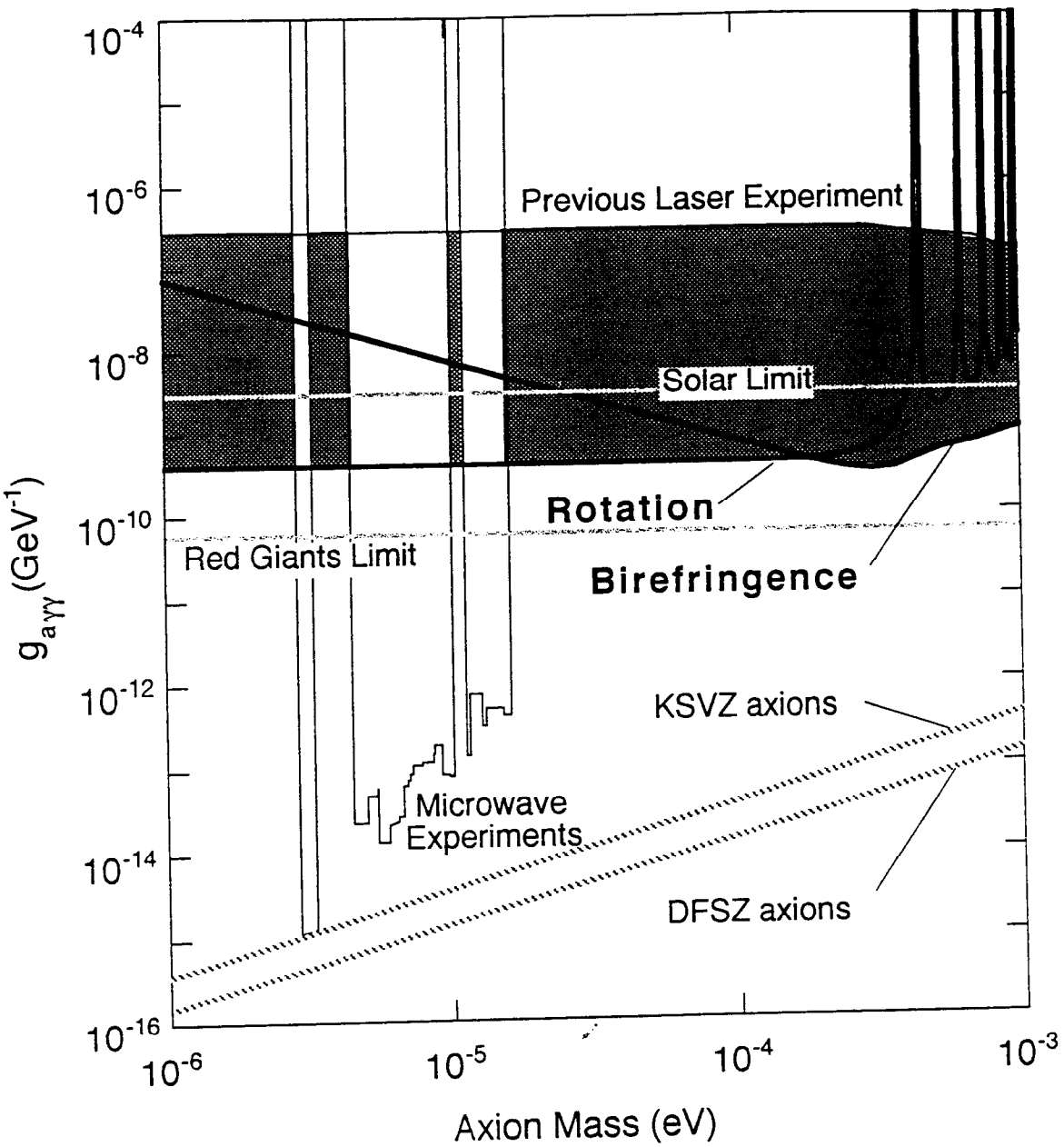

FIG. 2.3 Limits on axion mass and axion-two-photon coupling from experiments and astrophysical considerations. The dashed lines are the predicted relationship between $g_{a\gamma\gamma}$ and m_a for axions imbedded in GUT models. The gray lines are the astrophysical-based limits. The heavy solid lines are the sensitivity limits for the proposed birefringence and rotation experiments. The shaded area represents new experimental phase space to be probed by the proposed experiment.

The existing limits on axion-photon coupling within the 10^{-6} and 10^{-3} eV window are shown in Fig. 2.3. At the low end, microwave cavity experiments have reached the KSVZ axion GUT line in a narrow range 2.9-3.3 μeV [17] and have probed to within a factor of 50 of the GUT line in the broader range 4-16μeV. A basic assumption in these experiments is that the dark matter in the galactic halo is comprised of axions. An experiment to look for the conversion of solar axions into x-ray photons in a strong magnetic field provides a broad limit of $g_{a\gamma\gamma}<2.5\times10^{-9}$ GeV^{-1}. Axion mass independent astrophysical limits from the solar lifetime, $g_{a\gamma\gamma}<3\times10^{-9}$ GeV^{-1} and red giant evolution, $g_{a\gamma\gamma}<6\times10^{-11}$ GeV^{-1} are also shown.

The only laboratory axion search in this window, which is completely free of astrophysical arguments or assumptions, is the first-generation magnetic rotation, birefringence and photon regeneration experiment performed at Brookhaven National Laboratory in 1989-1992 [10,19]. A limit of $g_{a\gamma\gamma}<3.6\times10^{-7}$ GeV^{-1} for $m_a<10^{-3}$ eV was established in this experiment. However, the magnetic birefringence sensitivity was about five orders of magnitude short of the predicted QED signal.

The proposed experiment will be able to measure, at the photon shot noise level and averaging 56 hours of data, optical birefringence and rotation as low as $\psi_{min}= 3\times10^{-12}$ rad and $\epsilon_{min}= 8\times10^{-12}$ rad, respectively. The sensitivity improvements of about 5×10^{7} and 10^{6} over previous experiments will allow the new limits shown in Fig 2.3 to be reached. Clearly, the proposed experiment will not reach the GUT axion lines. Nevertheless, it will probe a substantial amount of phase space on the $g_{a\gamma\gamma}$ vs. m_a plot which has not been investigated by laboratory means. This is shown by the shaded region in Fig. 2.3. The limits for $g_{a\gamma\gamma}$ will be improved by more than three orders of magnitude compared to the first-generation experiment and will be within an order of magitude of the best astrophysical bounds established from the analysis of the evolution of red giant stars.

2.5 References

[1]. W. Heisenberg and H. Euler, Z. Physik **38**, 314 (1936). Other derivations have been made by V. Weisskopf in K. Danske Vidensk. Selsk. Mat.-fys. Medd. **14**, No. 6 (1936), and by J. Schwinger, Phys. Rev. **82**, 664 (1951).

[2]. S. L. Adler, Ann. Phys. (N. Y.) **67**, 599 (1971).

[3]. V. I. Ritus, Sov. Phys. JETP **42**, 774 (1976).

[4]. T. Kinoshita , "Theory of the Anomalous Magnetic Moment of the Electron - Numerical Approach", in T. Kinoshita, *Quantum Electrodynamics* (World Scientific, Singapore, 1990) p. 218-321.

[5]. T. Kinoshita and W. J. Marciano, "Theory of the Muon Anomalous Magnetic Moment ", in T. Kinoshita, *Quantum Electrodynamics* (World Scientific, Singapore, 1990) p.419-478.

[6]. P. Rullhusen, W. Muckenheim, F. Smend, M. Schumacher, G. P. A. Berg, K. Mork and L. Kissel, Phys. Rev. C **23**, 1375 (1981).

[7]. Proposed muon anomalous magnetic moment experiment at Brookhaven National Laboratory.

[8]. R. D. Peccei and H. Quinn, Phys. Rev. Letters **38**, 1440 (1977).

[9]. G. Raffelt and L. Stodolsky, Phys. Rev. D**37**, 1237 (1988).

[10]. Y. Semertzidis, R. Cameron, G. Cantatore, A. C. Melissinos, J. Rogers, H. J. Halama, A. Prodell, F. Nezrick, C. Rizzo and E. Zavattini, Phys. Rev. Lett. **64**, 2988 (1990).

[11]. M. S. Turner, "Windows on the Axion", Phys. Reports **197**, 67 (1990)

[12] G. G. Raffelt and D. S. P. Dearborn, Phys. Rev. D **36**, 2211 (1987). G. G. Raffelt, Phys. Rep. **198**, 1 (1990).

[13] M. A. Bershady, M. T. Ressell and M. S. Turner, Phys. Rev. Lett. **66**, 1398 (1991).

[14] M. S. Turner, Phys. Rev. Lett. **60**, 1797 (1988); R. Mayle et al., Phys. Lett. B **203**, 188 (1988); **219**, 515 (1989). W. Keil et al., Phys. Rev. D**56**, 2419 (1997).

[15]. C. Hagmann *et al.*, Rev. Sci. Instrum. **61**, 1076 (1990).

[16]. S. DePanfilis, A. C. Melissinos, B. E. Moskowitz, J. T. Rogers, Y. K. Semertzidis, W. U. Wuensch, H. J. Halama, A. G. Prodell, W. B. Fowler and F. A. Nezrick, Phys. Rev. Lett. **59**, 839 (1987); Phys. Rev. D **40**, 3153 (1989).

[17] C. Hagmann *et al.*, Phys. Rev. Lett. **80**, 2043 (1998).

[18] D. M. Lazarus, G. C. Smith, R. Cameron, A. C. Melissinor, G. Ruoso, Y. K. Semertzidis and F. A. Nezrick, Phys. Rev. Lett. **69**, 2333 (1992).

[19] R. Cameron, G. Cantatore, A. C. Melissinos, G. Ruoso, Y. Semertzidis, H. J. Halama, D. M. Lazarus, A. G. Prodell, F. Nezrick, C. Rizzo and E. Zavattini, Phys. Rev. D **47**, 3707 (1993).

3. EXPERIMENTAL METHOD

The main optical instrument is a 50 m interferometer and birefringence spectrometer that is sensitive to a differential index change of 7×10^{-25} (for a 0.5% QED experiment), has a dynamic range > 180 dB, and provides 25,000 passes through the use of a high finesse Fabry-Perot cavity. A simplified diagram of the proposed experiment is shown in Fig. 3.1. The output of a Nd:YAG laser is frequency-doubled and sent into a high-finesse Fabry-Perot cavity. A strong transverse magnetic field exists in most of the length of the cavity. The input laser polarization is at 45° to the B field. Each of the polarization components, parallel and perpendicular to the B field direction, is separately locked to its own cavity resonance by the Pound-Drever-Hall technique [1]. The phase difference between the two polarization components due to birefringence will be measured as a direct readout of the small frequency difference between them. The light transmitted from the cavity will be used for polarization rotation measurement in a standard polarimeter arrangement [2, 3]. Both the Fabry-Perot cavity and the birefringence spectrometer will be housed in a vacuum system with a pressure of 10^{-7} torr.

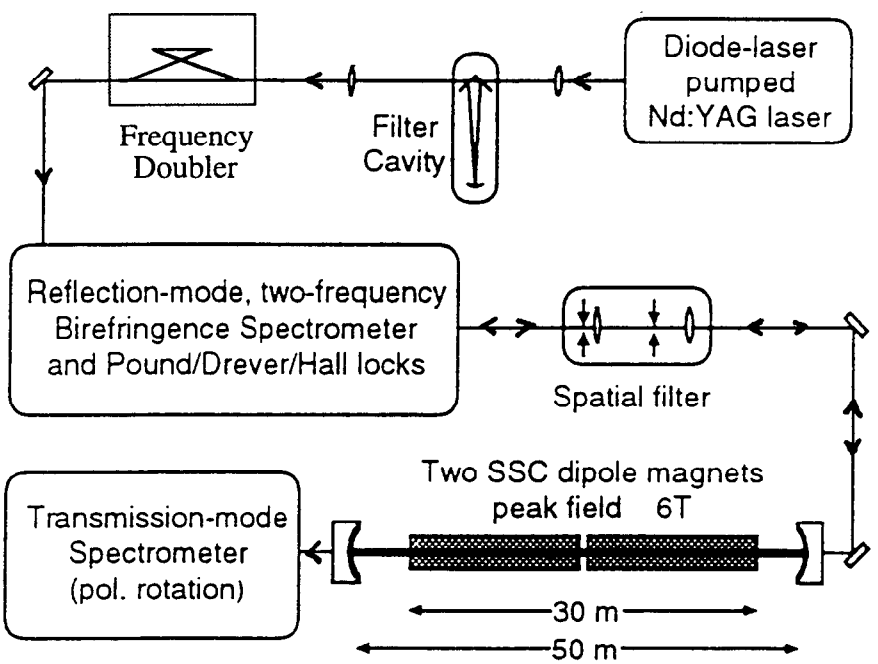

FIG. 3.1 Schematic optical configuration of the proposed experiment.

3.1 The Laser Source

The laser is a frequency-doubled, diode-pumped Nd:YAG laser. A filter cavity is used to narrow the laser linewidth [4] and to ensure the pointing stability of the laser beam. The absolute frequency of the laser is stabilized to a hyperfine structure in iodine. About 100 mW of 532 nm light will be delivered to the input of the main Fabry-Perot cavity.

3.2 The Magnets

The magnets are prototype dipole magnets developed for the ex-SSC. They have a peak field of 6.6 T, bore diameter of 3.8 cm, and length of 15 m. Two magnets are in the Fermilab E-4R facility. Based on previous SSC studies on these magnets, the magnetic field may be modulated from 1 T to 6 T at a modulation frequency of 5 mHz. Details of the magnets will be presented in Chapter 4.

3.3 The High Finesse Fabry-Perot Cavity

A Fabry-Perot cavity, formed by two mirrors, allows a light beam to reflect back and forth many times through the cavity. The interference between the multiply reflected beams produces the sharp frequency resonances of the cavity. The Fabry-Perot resonance condition is given by:

$$\frac{2\pi}{\lambda} 2nL + \phi_c = 2m\pi \qquad (3.1)$$

where m is an integer, n is the index of the medium in the cavity, L is the length of the cavity, λ is the vacuum wavelength of the light, and ϕ_c is the total of all other accumulated phase shift such as due to mirror reflection phase shift and birefringence, and weakly admixed higher order spatial modes. There is an additional constant phase due to diffraction. The resonance condition basically states that the total phase increment acquired through one round trip of light travel in the cavity should be equal to an integer number of 2π's.

On resonance, both the transmitted beam out of the back mirror and the reflected beam from the front mirror carry the phase information of the multipassed light beam. In the proposed experiment, the light will be polarized at 45° to the magnetic field direction. The // and the $\perp$ polarizations have slightly different refractive indices due to QED and possible axion induced birefringence. The ellipticity (defined as 1/2 the phase difference between the two polarizations)

accumulated in the reflected beam is

$$\psi = (2\frac{F}{\pi})\,\beta\,\psi_1 \qquad (3.2)$$

where F is the finesse of the cavity (defined as $\pi\sqrt{R}/(1-R)$, R being the mirror reflectivity), ψ_1 is the ellipticity acquired in a single pass through the magnetic field, and β is a constant ≈ 1 which is dependent on measurable mirror coating parameters. Eq (3.2) is written in such a form as to illustrate that the equivalent number of reflections in a Fabry-Perot cavity is

$$N \approx 2\frac{F}{\pi} \qquad (3.3)$$

Thus a large number of passes may be achieved with high finesse, i.e., a high mirror reflectivity. At the same time the scattering and absorption losses must be small enough to allow enough transmission through the cavity on resonance.

The design parameters for the 50 m Fabry-Perot interferometer are listed in Table 3.1. The mirror radius of curvature is chosen to minimize the mode size at the entrance and exit ends of the magnet bore. This will reduce stray light scattering from the magnet bore. The mirror diameter is determined from diffraction loss considerations. For the proposed interferometer, the diffractive loss for a TEM_{00} laser beam is estimated to be less than 10^{-13} for a 2" diameter mirror [5]. The finesse of the cavity is sufficiently high to allow detection of the QED induced birefringence. High reflectivity mirrors with total scattering and absorption losses below 5×10^{-6} are now commercially available [6]. To maintain such low losses, however, a clean environment (Class 10 or better) is needed during the assembly of the Fabry-Perot interferometer. In a semi-clean laboratory environment (Class 100), a more realistic loss figure is 15 ppm, and this value is used for designing the interferometer.

3.4 Seismic Isolation and Control of the Optical Interferometer

Ground motion contributes to motion of the cavity mirrors and can give rise to a frequency noise of more than 1 MHz, or $\sim 10^4$ linewidths of the cavity resonances. It is necessary to isolate the cavity from this seismic noise in order for the cavity to remain in resonance with the laser. The birefringence and rotation measuring optics will be mounted on inertial platforms

which are isolated from the vibrations of surroundings by passive and active means. The cavity mirrors are suspended from isolated platforms as the lower mass of double pendula to allow independent control of the tilt and axial motions of the mirrors. The passive seismic isolation ensures that high frequency ground motion is not communicated to the mirror. Active damping of the double pendulum motion keeps the cavity in near resonance with the optical frequency. Results from laser gravitational wave interferometers (LIGO and VIRGO projects [7, 8]) and in our collaboration show that passive vibration isolation and active mechanical damping of the mirror suspension will reduce the mirror motion to ~ 5 pm, or ~ 1 cavity linewidth. At this level, the feedback electronics will be able to follow residual mirror motions to keep the laser frequency in resonance with the cavity.

Total length of interferometer L	50 m
Total magnetic field region *l*	30 m
Mirror reflectivity R	0.99992
Mirror transmission T	6.5×10^{-5}
Finesse F	3.93×10^{4}
Equivalent number of passes N	2.5×10^{4}
Free spectral range	3.0 MHz
Cavity fringe full width half max	77 Hz
Mirror radius of curvature	34 m
Mirror diameter	5 cm (2")
Confocal parameter z_o	15 m
Minimum waist radius at 532 nm w_o	1.6 mm
Mode radius at mirror w	3.1 mm

Table 3.1 Parameters for the 50 m Fabry-Perot cavity

3.5 Birefringence Measurement

The basic scheme of the birefringence spectrometer is shown in Fig. 3.2. The incoming laser light is split into two paths with orthogonal polarizations. Two acousto-optic modulators (AOM 1 & 2) shift the frequency of the two channels independently. Each channel is frequency modulated with electro-optic modulators (EOM 1 & 2) which operate at different modulation frequencies. The two beams are recombined, sent through a rotatable half-wave plate, and mode-matched into the high finesse Fabry-Perot cavity. Additional optics are used to provide optical isolation and to ensure the proper polarization states for the laser beam when entering the cavity.

The frequency of each polarization component is separately locked to be on resonance with the Fabry-Perot cavity via the Pound-Drever-Hall FM locking scheme [1]. In this method, the incoming laser light is frequency modulated such that the fundamental mode is in resonance with the cavity, but the modulation sidebands are reflected by the cavity. The reflected beams are demodulated to provide a feed-back signal for keeping the laser in resonance. The frequency difference between the two polarizations is obtained from Eq. (3.1):

$$\Delta\nu = \nu_{\perp} - \nu_{/\!/} = \frac{c}{2n_o L}\left[m\left(\frac{\Delta n}{n_o}\right) + \frac{\Delta\phi_c}{2m\pi}\right] \qquad (3.4)$$

where n_o is the index with no magnetic field ($n_o = 1$ for a perfect vacuum), m is the order of the Fabry-Perot resonance, and c/2L is the free spectral range of the cavity. The first term in the bracket is due to the QED index difference, $\Delta n = n_{/\!/} - n_{\perp}$, as light propagates in the cavity. For the proposed experiment this term gives a frequency difference of 80 nHz. The second term accounts for other optical phase shifts such as that due to the birefringence in the mirror coatings. In studies carried out in our collaboration, it was found that the mirror coatings introduce a static birefringence of a few μrad. Thus the second term in Eq (3.4) contributes a dc signal at the Hz level. This static birefringence may be reduced by careful mounting and positioning of the mirror birefringence eigen-axes.

The two frequencies driving the acousto-optic modulators (AOM1 and AOM2 of Fig 3.2) will be derived from a common source, and direct digital synthesis (DDS) will be used to reduce the Hz level background to within the μHz step size of the DDS. The cavity lock error signal can then be divided into 1000 parts to reach nHz resolution. Calibration of the error signal is

accomplished by offsetting the DDS by a few μHz and noting the cavity response.

When the two polarization components are locked to the same cavity order in the manner described above, the seismic motions of the cavity mirrors produce common-mode noise and are greatly suppressed. However, the frequency difference is only at the Hz level due to the static birefringence of the mirror coatings. This small frequency difference is not ideal from a measurement point of view. The moderate intracavity power (~ 900 W in our case) may still lead to heating of the mirrors due to ppm level of absorption by the coatings. This results in a thermally induced birefringence. In addition, we have observed that the two polarization modes can interact with each other and produce a birefringence even at very low powers (< 1W), probably through a photo-refractive type response in the mirror coatings. These light related dynamic effects were much reduced when circularly polarized light was used.

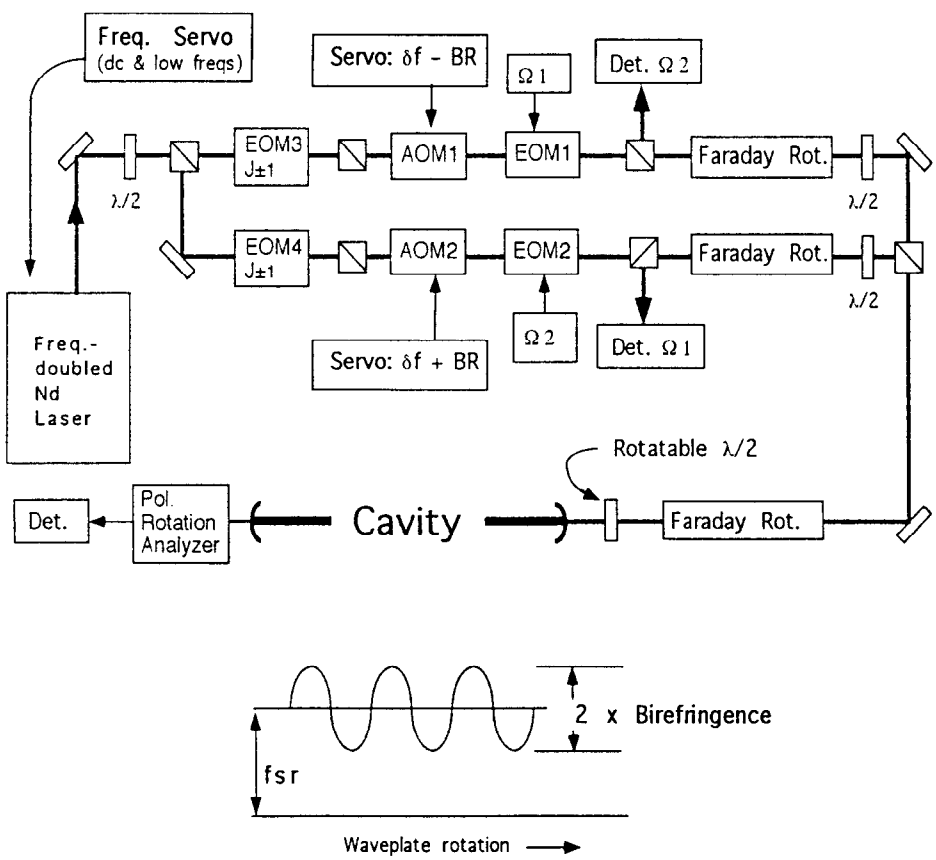

FIG. 3.2 Measurement scheme for the birefringent spectrometer. A direct measurement of the frequency difference between the two polarization components of the laser light gives the birefringence of light travelling in the Fabry-Perot cavity.

In view of the heating and polarization interaction problems, it is more advantageous to have a larger frequency interval between the two polarizations, so that there is a changing resultant E vector on the mirrors. One choice is to lock the two polarizations on different cavity modes. However, the seismic common mode characteristic is lost in this arrangement because the two modes no longer have the same wavelengths. We propose a solution which restores the common mode seismic suppression while maintaining a frequency difference between the two polarizations. This is achieved by using EOMs 3 & 4 to shift one polarized component (e.g., the // component) into two frequencies, one upshifted and the other one downshifted by exactly one cavity free spectral range from the original beam. Now the Pound-Drever-Hall lock system for the // component produces a cavity-lock signal which is based on the average of the two frequencies. This error signal will be compared to the error signal from the $\perp$ component, and the result is free of seismic noise. The exact frequency supplied to these EOM's is not critical (~ to within 1 Hz of the cavity FSR) and can be refined by measurements in an additional rf detection channel as described by DeVoe et al. [9].

A rotating wave plate will be used to change the polarization of the light incident to the cavity. This allows synchronous detection of the birefringence at a frequency much higher than the 5 mHz ramp rate of the magnets. A preliminary investigation of measuring small phase differences in a high finesse Fabry-Perot cavity will be discussed in Section 8.1.

3.6 Rotation Measurement - A Means to Search for Light Scalar or Pseudoscalar Particles

In the presence of a strong magnetic field, an axion creation event would lead to a small absorption of the laser field component polarized parallel to the static magnetic field. If the light beam is polarized at 45° to the magnetic field direction, such a preferential absorption of one polarization component would lead to a small rotation in the polarization vector of the recombined beams. The rotation measurement method will be similar to that of a previous experiment by Cameron et al. [3]. An analyzer is oriented such that its transmission axis is orthogonal to the original polarization axis of the main beam. A small rotation ε in the polarization then leads to a transmission intensity proportional to ε^2 through the crossed analyzer. To obtain higher sensitivity, a much larger, sinusoidally modulated rotation $\eta(t)$ is introduced by a Faraday cell before the analyzer. Heterodyne detection then produces an interference term $\eta\varepsilon$

in the transmitted intensity which is linear in ε. One minor difference in our experiment is that the cavity finesse is very high and the two polarization modes will have slightly different resonance frequencies. So the phase of the two transmitted polarization components will be differentially delayed by ~ 2 $\tan^{-1}$ (Δν/cavity width) = 2 $\tan^{-1}$ (2 Hz / 77 Hz) = 52 mrad or about 3°. However, a stable phase compensator, such as a Babinet-Soleil compensator, will restore the perfect phase equality, and hence we will still have the very dark null when looking through the crossed analyzer.

3.7 Evaluation of the Shot Noise Limited Performance of the Interferometer

3.7.1 Birefringence Measurement Shot Noise Limit

For the QED birefringence experiment, measurements will be made with the reflected beams from the Fabry-Perot interferometer. In the Pound-Drever-Hall (PDH) locking scheme [1], the incident laser beam is frequency modulated at frequency Ω with a modulation index m, and the incident electric field to the cavity may be written as

$$E=E_i\,[J_o(m)\cos(\omega t)+J_1(m)\cos(\omega+\Omega)\,t-J_1(m)\cos(\omega-\Omega)\,t] \qquad (3.5)$$

where ω is the optical frequency and the J(m)'s are Bessel functions with argument m. Higher order harmonics are neglected in the above equation. The FM frequency Ω is chosen such that, on resonance, only the fundamental frequency (the J_o term) is transmitted into the cavity and the side bands are reflected. In other words, Ω should be >> the cavity linewidth.

In this experiment we are measuring the current in a photodetector when light is incident on it. The statistical fluctuations due to the random emission of photoelectrons (i.e., the shot-noise) produce a noise current given by

$$i_n=\sqrt{2\,e\,i_{dc}\,B} \qquad (3.6)$$

where i_{dc} is the photodetector current, e is the charge of the electron, and B is the bandwidth of detection. When the cavity is on resonance, the reflected fundamental beam experiences destructive interference, and the photocurrent is mainly due to the reflected sidebands and residual fundamental light from imperfect contrast of the dark fringe. A typical conversion factor

between optical power and photocurrent at 532 nm is η = 0.3 mA/mW. Thus, for reflected beam on resonance, $i_{dc}=\eta P_r$, where P_r is the reflected power given by

$$P_r = [1-J_o^2(1-R(\frac{1-R-T}{1-R})^2)]\,P_i \qquad (3.7)$$

The slope of the PDH discrimination curve provides the conversion factor from signal photocurrent to optical phase change. A signal current of $\eta \cdot 2J_oJ_1P_i$ is equivalent to a single pass induced ellipticity of $(\pi/4F)(1-R)/T$ radians. Since the number of passes in a cavity is given by $N=2F/\pi$ (Eq. 3.3), the shot-noise limited, minimum detectable ellipticity is

$$(\psi_{min})_{BR} = [\frac{1-R}{2T}]\frac{\sqrt{2e\eta P_r}}{2\eta J_oJ_1P_i} \quad rad/\sqrt{Hz} \qquad (3.8)$$

For consideration of shot-noise limited performance, we assume an incident power P_i = 100 mW to the cavity, and a modulation index m = 0.5. With mirrors of transmission T = 6.5×10^{-5} and loss L = 1.5×10^{-5}, the reflected power on resonance is calculated from Eq. (3.7) to be 15 mW. The transmitted power is $P_t = [J_oT/(1-R)]^2P_i$ = 58 mW, and the power circulating inside the cavity is P_t/T= 894 W. We also note that the incident laser power is split equally between the two polarizations. We need to keep track of them separately, and add their shot noise contributions in quadrature. In terms of spectral density, our analysis shows that the shot noise limited sensitivity for ellipticity detection is 3.3 x 10^{-9} rad /$\sqrt{}$Hz. A 48 hour integration at the shot-noise limit will give $\psi = 3.2\times10^{-12}$ rad, which is 0.5% of the calculated QED value of 6.3×10^{-10} rad.

3.7.2 Rotation Measurement Shot Noise Limit

The rotation measurement uses the transmitted beam from the cavity. The experimental approach is similar to the previous experiment [3] and the shot noise limited performance is comparable. A detailed analysis of our system gives a shot-noise limited rotation sensitivity of 9×10^{-9} rad/$\sqrt{}$Hz, about a factor of two worse than in Ref. 3. The 10^4 improvement in sensitivity in our proposed experiment over the previous experiment comes mainly from the increased number of passes, a longer B field region and higher field strength.

3.8 References

[1]. R. W. P. Drever, J. L. Hall, F. V. Kowalski and J. Hough, G. M. Ford, A. J. Munley and H. Ward, Appl. Phys. B **31**, 97 (1983).

[2] Y. Semertzidis, R. Cameron, G. Cantatore, A. C. Melissinos, J. Rogers, H. J. Halama, A. Prodell, F. Nezrick, C. Rizzo and E. Zavattini, Phys. Rev. Lett. **64**, 2988 (1990).

[3] R. Cameron, G. Cantatore, A. C. Melissinos, G. Ruoso, Y. Semertzidis, H. J. Halama, D. M. Lazarus, A. G. Prodell, F. Nezrick, C. Rizzo and E. Zavattini, Phys. Rev. D **47**, 3707 (1993).

[4] Ch. Salamon, D. Hils and J. L. Hall, J. Opt. Soc. Am. B **5**, 1576 (1988).

[5] H. Kogelnik and T. Li, App. Opt. **5**, 1550 (1966).

[6] G. Rempe, R. J. Thompson, H. J. Kimble and R. Lalezari, Opt. Lett. **17**, 363 (1992).

[7] A. Abramovici *et al.*, Science **256**, 325 (1992); A. Gillespie and F. Raab, Phys. Lett. A **178**, 357 (1993); the LIGO web site at www.ligo.caltech.edu.

[8] B. Caron *et al.*, "VIRGO: A wideband gravitational wave detector," LAPP-EXP 96.10. S. Braccini *et al.*, Rev. Sci. Instrum. **67**, 2899 (1996); the VIRGO website at www.pg.infn.it/virgo/.

[9] R. G. DeVoe, C. Fabre, K. Jungmann, J. Hoffnagle and R. G. Brewer, Phys. Rev. A **37**, 1802 (1988).

4. MAGNET SYSTEM

4.1 Magnet System Requirements

To maximize the QED signal for this experiment, the dipole magnet system must (1) deliver a high value of magnetic field over a long length, (2) be capable of modulation, (3) have a sufficiently large aperture, (4) have an aperture tube which can achieve an ultra high vacuum, and (5) exist as tested complete magnets. These requirements are met with dipole magnets that were constructed for the SSC.

The individual SSC dipole magnets which we considered were those which have been thoroughly tested. Extensive measurements were made for ramp rate dependence on quench current, AC losses, total heat load, magnetic field transfer function and mechanical behavior. Based on these data the magnet system requirements and characteristics were determined and are presented in Table 4.1. The desired 30 m length of magnetic field is achieved by using two 15 m SSC prototype dipole magnets. The proposed magnetic field ramping is from 1 T (1000 A) to 6 T (6000 A) at 100 A/s. The magnetic field modulation cycle will be trapezoidal with a 50 s up ramp, 50 s plateau, 50 s down ramp, and a 50 s dwell at 1000 A. The modulation frequency is 5 mHz.

4.2 Magnet Selection

From the SSC inventory of nearly two dozen prototype dipole magnets, two 15 m dipoles magnets plus one spare were selected which best matched the criteria of Table 4.1. These magnets are DCA207, DCA209, and DCA318 respectively. The dominant magnet properties relevant to this experiment are quench performance, ramp rate behavior, and AC losses.

The current at which a superconducting magnet will quench is a function of the current ramp rate, the operating temperature, and the amount of cooling (He mass flow). At 4.3 K and 50 g/s He flow, most SSC prototype dipoles built at FNAL and BNL achieved quench currents in excess of 6000 A (6T) at 100 A/s ramp rate. Almost all magnets achieved 300 A/s for their down-ramp. The three magnets chosen for this experiment have the quench current vs. ramp rate dependence given in Fig. 4.1. Magnets DCA207 and DCA209 were measured with a He mass flow of 100 g/s while magnet DCA318 was measured at 50 g/s.

Dipole Magnet Length (end plate to end plate)	15.3 m
Magnetic Field Modulation	1 to 6 Tesla
Ramp Rate	100 A/s
Dipole Field Measurement Accuracy Error	< 1%
Beam Tube Clear Aperture	38 mm
System Inlet He Temperature	4.35 K
Length of Magnet Interconnect Region	1.2 m
Inductance per Magnet	76 mH
Power Supply Output Current (max.)	7,000 A
Power Supply Output Voltage (max.)	40 V

Table 4.1 Magnet System Parameters and Requirements

The values of quench current as a function of ramp rate given in Fig 4.1 are for an operating temperature of 4.3 K. If the operating temperature of the magnets is decreased, the quench current will increase by 18%/K. [1].

The AC loss, a measure of the total energy deposited in the magnet during current ramping, is dependent on the superconductor hysteresis loss, yoke material, and eddy current heating in the magnet coil. For the magnets selected the hysteresis losses are about 740 Joules per cycle and the eddy current losses are about 11 W/A per cycle, giving a total losses per magnet of about 22 Watts at a ramp rate of 100 A/s.

4.3 Magnetic Field Issues

For the SSC dipoles the transfer function (ratio of magnetic field to coil current) between 2000 A and 5000 A is 1.044 T/kA and linear to 0.1%. At 5 T the iron yoke becomes magnetically saturated. At 6 T the transfer function is lowered by about 2%. The magnetic field harmonics of the selected magnets have been measured [2] but are unimportant for this experiment. The magnets were thermally cycled twice to room temperature and remeasured. There is sufficient data to convince us that the mechanical design and quench performance of

these magnets have not been affected by thermal cycles, repeated excitation, and quenching at high currents. It is unlikely that continuous ramping of the magnets between 1 and 6 kA will have any ill effects on the mechanical structure and electrical integrity of these magnets.

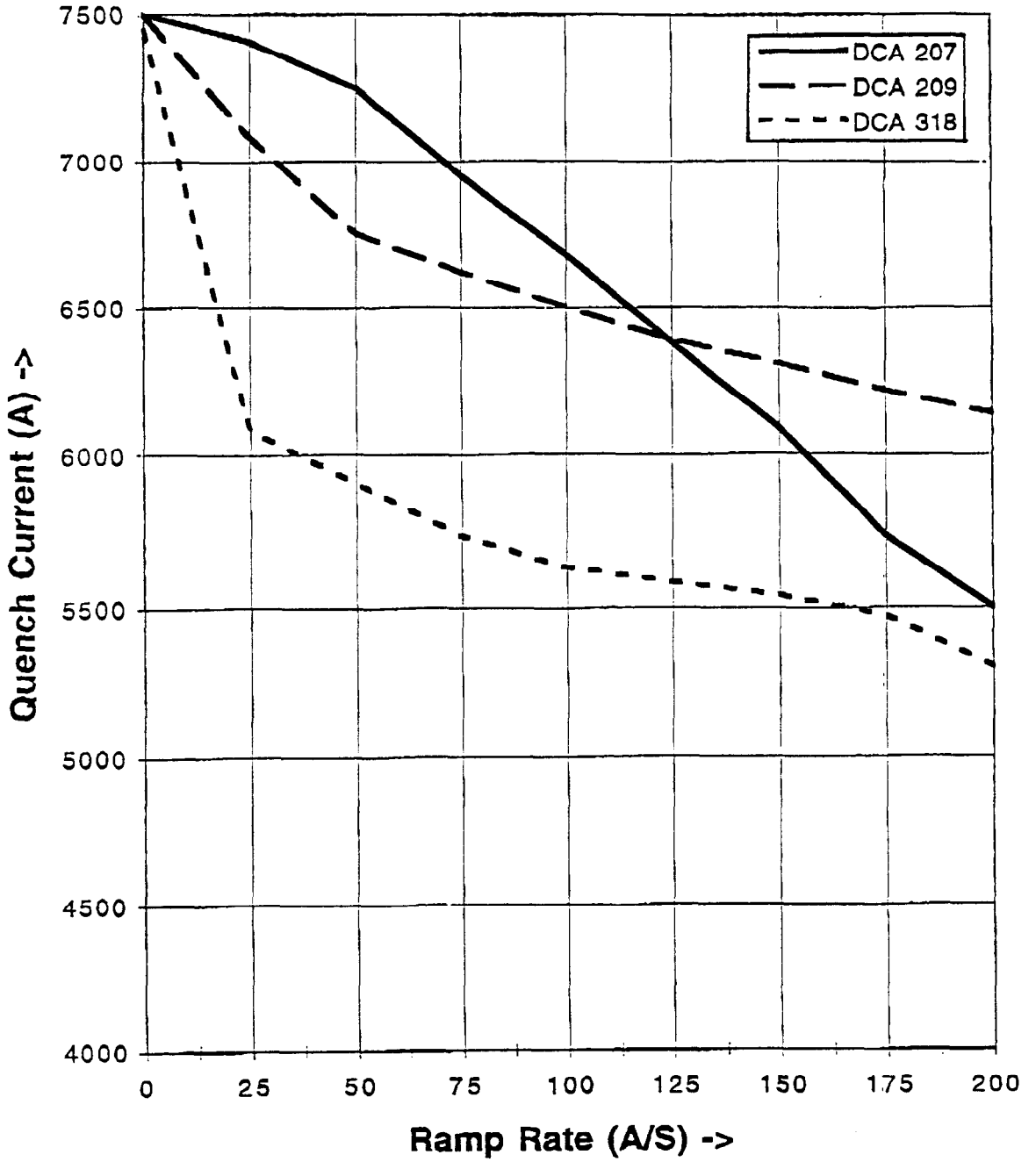

FIG. 4.1 Ramp rate dependence of quench current.

4.4 Cryogenic Considerations

The cryogenic system must carry away the static and dynamic heat produced by the modulating magnetic field system. Three cooling loops, at 4 K, 20 K and 80 K, are used with the magnets. Table 4.2 lists the total heat loads for a two dipole magnet system for each of the three cooling loops. The heat load values used for the dipoles are from measurements at SSC. The head load values for the end cans are based on Fermilab testing of 40 mm bore SSC dipoles at E-4R.

If the entire heat load is transferred to the He, then the temperature rise, dT, across each element is given by dT=Q/mC, where Q is the heat load of the element (W), m is the mass flow of He (g/s) and C is the specific heat for liquid He at 4.3K (3.95 J/g-K). If the He input temperature is 4.35 K and the mass flow is 50 g/s, then the total temperature increase is 0.02 K across an end can and 0.12 K across a single magnet. The He temperature exiting the second dipole is 4.61 K. This temperature rise appears to be acceptable for ramping the magnets at 100 A/sec to 6000 A.

	4 K	**20 K**	**80 K**
	Watts	Watts	Watt
Magnet System Static Heat Load			
Single Dipole	(1.5)	(5.6)	(37)
Two Dipoles	3	12	74
Feed End Can	5	5	0
Return End Can	5	5	0
Total Static Heat Load	13	22	74
Magnet System Dynamic Heat Load			
Single Dipole	(22)	0	0
Two Dipoles	44	0	0
Total Dynamic Heat Load	44	0	0
Magnet System Total Heat Load	**57**	**22**	**74**

Table 4.2 Heat Loads for a Two Magnet System in the 4 K, 20 K and 80 K Cooling Loops

4.5 Power System Requirements

This experiment requires high ramp rates (100 A/s) and continuous cyclic operations between 1000 A and 6000 A, for testing and data taking periods of a few weeks to a month with a high degree of reliability. It is proposed that the Main Injector prototype power supply facility at E-4R will be used to power the magnets in this experiment. The magnet system requires 6000 A at 40 V to meet the requirements given in Table 4.1. The E-4R facility, which has operated reliably for several years, can provide a maximum of 9500 A at 1000 V. Water cooled conductors will connect the power supply to the magnet system. It appears that the existing power supply control system is adequate to provide the phase locked current wave form and other controls required for this experiment.

4.6 Quench Protection System

The power supply and quench protection system (QPS) must function together as an integrated system. If a section of the superconducting system starts to go normal, then the QPS senses the impedance change and "disconnects" the power supply from the magnet system and fires the heater firing unit (HFU). The HFU powers the heater strips in each of the two magnets, which drives both magnet coils normal and allows the quench energy to be dissipated over a larger volume of superconductor. It is believed that with a two magnet system a quench bypass system and a power dump are not required. The experiment will use existing Fermilab QPS units and HFUs.

4.7 Optics and Magnet System Interface

The beam tube installed in the dipole magnets selected for this experiment has an internal diameter of 42±0.14 mm, wall thickness of 1.3 mm, and is made of Armco Nitronic-40 stainless steel. There is no sagitta in these magnets. The cold masses are known to have some sag (~0.02 mm) which is a function of the magnet current [3,4], and the beam tube position can vary within the 50 mm coil aperture. There is also a slight misalignment between the beam tubes of the magnets and the beam tubes in the cryogenic end cans.

If the problem of photodesorption of H_2 in the beam pipe is serious (see Section 7.1), then additional vacuum pumping and residual gas analysis must be provided at the interconnect region between the two dipoles. This is a contingency plan to be determined by photodesorption

measurements of the actual beam tube.

The magnet system feed and return cans provide the interface volume between the power and cryogenic systems and the magnets. The optical access to the magnetic field region is via the beam tube which passes through the feed and end cans. In the feed and end cans the beam tube has an 80 K shield to minimize heat transfer into the 4.3 K magnet beam tube. UHV gate valves outside the feed and end cans will isolate the cold vacuum region.

A low profile stand to support and align two dipole magnets and two end cans was designed for the SSC magnet measuring facility and is acceptable for the preliminary phase of this experiment. Improvements in the stand if necessary could include automatic magnet alignment to maximize the clear aperture, and passive vibration isolation to minimize the noise contribution from light scattered from the magnet beam pipe (see Section 7.2).

4.8 Technical Risks and Mitigation

The major technical risks within the magnet system involve those aspects which can not be evaluated by measurements on individual magnets. Will the magnet system ramp at 100 A/s to 6000 A repeatedly and reliably? Deficiencies in this area can be mitigated by increasing the He mass flow and/or decreasing the temperature of the He input. Does the magnet system have an adequate clear aperture? If the individual elements have an adequate aperture then the system aperture can be optimized by proper and active alignment. Possible misalignments which develop as a function of magnet excitation are more problematic. Risks associated with beam tube seismic vibrations are discussed in Section 7.2. Each of the magnets selected for this experiment has been individually tested at the Fermilab Magnet Test Facility.

4.9 References

[1] T. Jaffery, *et al.* "Test Results of Post-ASST design Fermilab-Built 1.5 m SSC Collider Model Dipoles", IEEE Trans. Appl. Superconductivity, **2**, 666 (March 1993).

[2] T. S. Jaffery, M. Wake and W. Kinney, "Automated Methods of Field Harmonics Extraction and Processing for the Magnets in Superconducting Super Collider", presented in International Measurement Technology Conference, Hamamatsu, Japan, May 10-12, 1994.

[3] J. Strait, *et al.*, "Mechanical Design of 2D Cross-section of the SSC Collider Dipole

Magnet", IEEE Particle Accelerator Conference, San Francisco, CA, May 6-9 1991. 4, 2176 (1991).

[4] E. G. Pewitt ed. "50 mm Collider Dipole Magnet Requirements and Specifications", Fermilab 16 Aug. 1991.

5. VACUUM SYSTEM

The vacuum system for the interferometer consists of three regions; the magnet beam tube region, the two optical chambers which house the interferometer mirrors, and the differentially pumped transition sections between the magnet beam tube and the optical chambers. The magnet beam tube operates at 4.3 K while the remaining parts of the vacuum system operate at room temperature. Several considerations are important for the design of the vacuum system. The residual gas in the magnet beam tube can produce optical birefringence and optical polarization rotation through the Cotton-Mouton (CM) effect and the Faraday effect, respectively. Therefore achieving ultra low vacuum in the magnet beam tube is a critical concern of the experiment. The requirement of very low scattered laser light in the interferometer necessitates careful consideration of the design and materials for a baffle system and possible liner within the magnet vacuum beam tube. Light traps and additional baffles in the interconnecting region between the magnets and in the transition regions are also needed. Vibration isolation of the optics and active control of the motion of the interferometer mirrors impact the vacuum in the optical chambers. Shielding the optics from background magnetic fields must also be achieved. Since the three regions have different vacuum requirements, each will be discussed separately.

5.1 Magnet Beam Tube Region

The magnet beam tube region of the vacuum pipe is cryopumped by the cold bore of the super-conducting magnets. At 4.2 K the only gases remaining should be H_2 and He. Because this region has a high magnetic field, these gases will introduce systematic errors in the optical birefringence and rotation measurements through the Cotton-Mouton (CM) effect and the Faraday effect. A birefringence at the shot noise limit, $\Delta n_{shot}=7\times10^{-25}$ can arise through the CM effect from a H_2 density of 1×10^{6} molecules/cm^3 (4×10^{-13} torr partial pressure at 4.2 K) within the magnet beam tube. We therefore set the design pressure for the magnet beam tube region at 4×10^{-13} torr. Although the starting base pressure at 4.2 K in the beam tube can be better than this [1], the base pressure can degrade due to the photodesorption of H_2 by scattered laser light and outgassing from the warmer parts of the vacuum system. The CM effect, the Faraday effect, and the H_2 problem are discussed in detail in Section 7.1. The conclusions from that section are that the

vacuum capability, as these magnets now stand, is far from adequate. These magnets were prototypes and were not prepared to go into an accelerator. The beam tube was neither heat treated nor polished or coated. A perforated liner with cryosorbing material is under study to control the H_2 density. The liner can be designed to also act as a light absorber, thereby reducing the multiple scattering of light in the magnet beam tube.

A larger bore vacuum tube (at least 10 cm in diameter) containing a Ti sublimation pumping system is to be installed in the interconnect region between the dipole magnets. In this section a portion of the gases generated in the cold bore region will be pumped away. If a penetration from the beam tube (4 K) to the outside (300 K) is installed in the interconnect region, then a residual gas analyzer will be installed in this region to aid in detecting the photodesorption contamination of the vacuum. This will be undertaken only if detailed testing indicates it is required. Another important role of the large bore vacuum tube is to allow light baffles to be placed at properly designed angles so that the pump section acts as a light trap. Our design philosophy is to direct as much of the scattered light as possible into the interconnect regions between the magnets. There the magnetic field is low, absorption of stray light can be efficient on blackened surfaces, and the pumping speed is high. In this way the release of H_2 molecules within the magnet bore regions can be minimized.

5.2 Optical Chambers

The optical chambers house the interferometer mirrors and their seismic vibration isolated suspension systems. The vacuum requirement for the optical chambers is not as stringent as for the magnet beam tube region. Since the magnetic field will be shielded to a very low value in these regions, the CM and Faraday effects are not a concern. A vacuum of $\leq 10^{-7}$ torr should be adequate to keep the interferometer mirrors sufficiently clean to maintain their low losses and to avoid significant coupling of acoustic perturbations through the residual gas in the chamber .

Each optical chamber will consist of an UHV vacuum chamber 36" in diameter and 126" high. As illustrated in Fig. 5.1, the chamber is divided into three sections so that the top two sections can be removed to allow easy access to the seismic isolation system and the optics housed within the chamber. The bottom section of the optical chamber will be anchored to earth and will be connected to the interferometer beam tube. The seismic vibration isolation system

for the interferometer mirror consists of passive and active stages. The passive stages are patterned after the systems designed for the gravitational wave experiments LIGO [2], VIRGO [3] and GEO [4]. The stages under development consists of a 2 m inverted pendulum supporting a torsion-crank-linkage super spring and conventional pendulum which supports the interferometer mirror [5]. The passive isolation system is supported by horizontal beams which pass through the vacuum chamber and anchor to the ground. Soft bellows provide the vacuum seal around the support beams. This arrangement ensures that rapid ground motion is not transmitted to the optics and the interferometer mirrors. The laser beam enters the vacuum chamber through an optical fiber. Actively steered mirrors could replace the fiber if necessary. There are no optical windows between the interferometer mirrors in order to minimize loss and scattering in the high-finesse interferometer cavity.

The optical chambers will be pumped out initially with a turbopump. The operating pressure will be maintained with vibration-free ion and Ti-sublimation pumps. Even with the large number of optical components and associated servo control wiring, a pressure of $\leq 10^{-7}$ torr should be readily achievable in the optical chambers. With specially designed vacuum compatible optical components and careful choice of material for wiring and vibration isolation, it is reasonable to expect that a vacuum of 10^{-9} torr can be achieved. The extensive experience of the LIGO and VIRGO projects in this area will be an advantage.

5.3 Differentially Pumped Regions

A transition region must be provided between the room temperature optical chambers at 10^{-7} to 10^{-9} torr and the ultra-high vacuum region ($\leq 10^{-12}$ torr) of the magnet cold bore. This will be provided by a series of differentially pumped sections. The primary concern is molecules which travel down the center of the beam tube on ballistic trajectories. The mirrors serve as obstacles, blocking the direct paths of gas molecules from the optical chambers to the bore. The gases generated in the interface region will be pumped by small ion pumps and large area getters from Ti sublimation pumps or other materials. The proper design and performance of this transition region is critical to the success of the experiment.

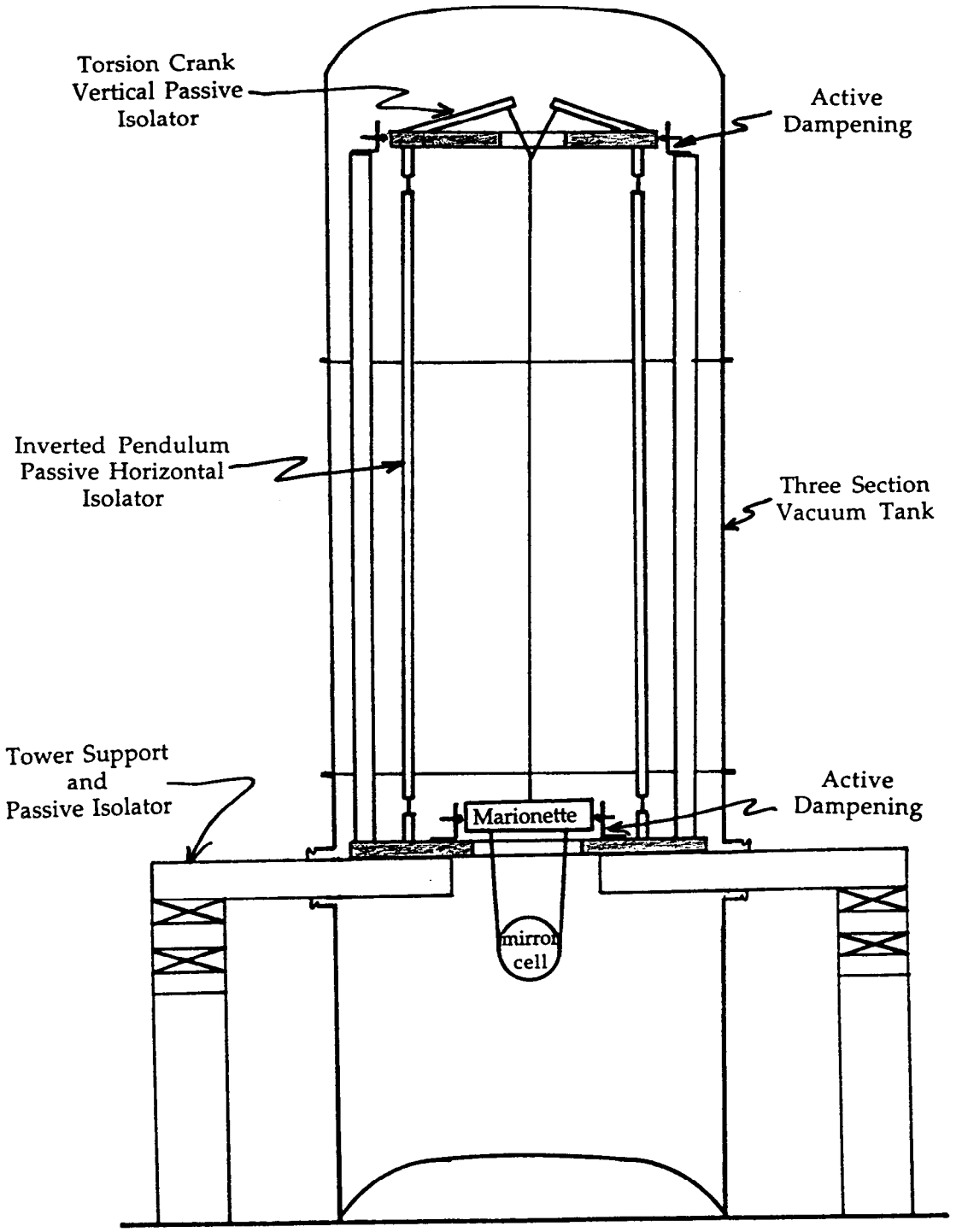

FIG. 5.1 Scheme under development for active and passive seismic vibration isolation for interferometer mirrors at each end of the magnet string.

5.4 References

[1]. William Turner, private communication.

[2]. The LIGO web site at www.ligo.caltech.edu.

[3]. The VIRGO web site at www.pg.infn.it/virgo/.

[4]. M. Plissi, *et al.*, Rev. Sci. Instrum. **69**, 3055 (1998). The GEO web site at www.GEO600.uni-hannover.de/.

[5]. F. Nezrick, "Measuring the effect of a magnetic field on the speed of light in vacuum" to be published in proceedings of "Frontier tests of QED and physics of the vacuum". Sandansky, Bulgaria, 9-15 June, 1998.

6. PHYSICAL PLANT AND ENVIRONMENTAL CONTROLS

6.1 Location of Experiment

The physical location of the experiment is dictated by the following requirements. First, the appropriate cryogenics services and magnet power must exist to operate the two SSC dipole magnets in a ramping mode, to a peak magnetic field of 6T. Second, the structure must have a length of at least 70m to house the interferometer. Third, the location should be somewhat removed from major ground vibration sources such as the Central Helium Liquefier. These conditions were met by the existing SSC magnet string test facility at E-4R. The cryogenics and power supply still exist at the E-4R pole building. The refurbished test string enclosure adequately houses the interferometer and magnets. See Fig. 6.1. The control portakamp suffices as the electronics counting room.

6.2 Magnet Enclosure

The two 15 m SSC dipole magnets are housed in a cast concrete structure composed of 10 Fermilab Main Ring tunnel hoops. Each Main Ring tunnel hoop has internal dimensions 11 ft wide by 9 ft high by 10 ft in length. The cryogenic end cans, because of their height and additional space required for cryogenic U-tube insertion, are located in rooms which are 14 feet wide by 14 feet high by 20 feet long. These enlarged rooms are the optics rooms of Section 6.3. The ground seismic vibration noises is kept to a minimum by the use of a floating slab construction. There is no requirement on the cleanliness of the air in the magnet enclosure, although the air should be dehumidified. This area will be an ODH area with ventilation provided through the optics rooms. The magnet enclosure will be accessed through the optics rooms.

6.3 Optics Rooms

The optics rooms are located at each end of the magnet enclosure. They house the large optical vacuum chambers, the optical tables supporting the laser and external optics, and vacuum pumping system. To decouple the floor motion caused by the modulating magnets from the optical systems, the optical vacuum chambers and optical tables are mounted on concrete floors

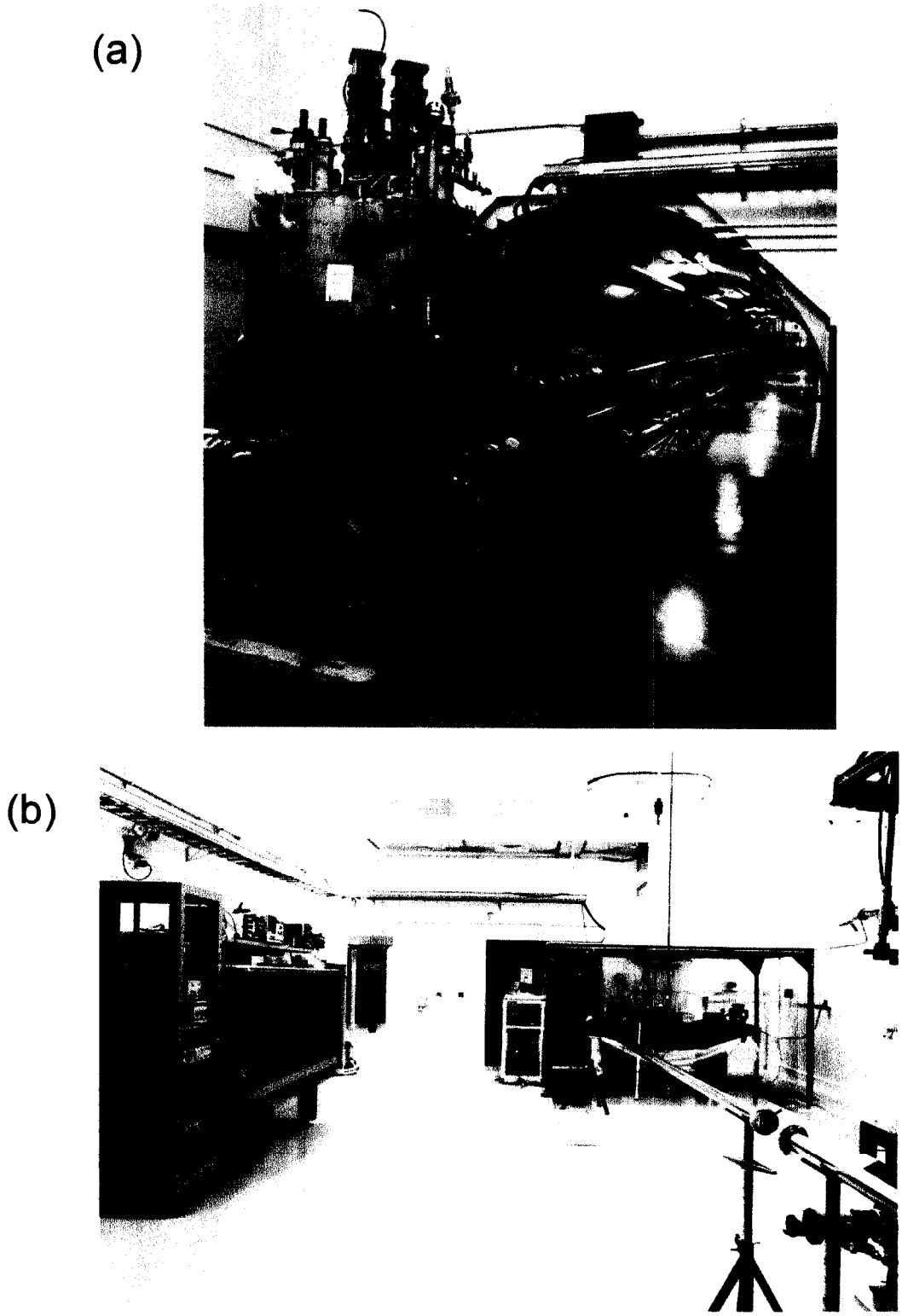

FIG. 6.1 Experimental facility at E4-R. (a) Magnet tunnel with the two SSC prototype magnets installed. The feedcan in the foreground is in the Center Hall. (b) Center Hall optics room.

floating in sand. The optics rooms are designated E-4R-Center and E-4R-South. These two rooms have different space requirements. E-4R-Center will be the primary laboratory for the experiment housing the main laser and optical analysis systems and the magnet cryogenic and power feed systems.

Each optics room is comparable to a Class 10,000 clean room. To maintain the optics rooms at a Class 10,000 level it is necessary that they have controlled access to the outside areas through air interlocks. The optical tables in the rooms are maintained at a clean room level of Class 100. In addition, when the optical vacuum chambers are opened their interior must be maintained at a class 100 level. For ultra-clean sub-assembly work it is our intent to request use of the Research Division Class 10 clean room in the village.

6.4 Counting and Control Room

A counting room with work area and office space is available which serves as an assembly area for mechanical and optical subsystems, and for electronics , computers and safety systems needed for the safe control of the system and for system development. The counting room also serve as an environmental intercept between the outside prairie and the clean room quality optics halls.

6.5 Cryogenics Requirements

A nominal He flow of 50 g/s at an inlet temperature of 4.35 K and pressure of 4 atm is required for proper operation of the two SSC dipole system. He gas at 20 K and LN_2 at 80 K are needed to maintain the heat shields of the magnet. These gasses are available from E-4. No cryogenics is transferred into E-4R at the present time. Cryogenic transfer lines, transition boxes and stingers exist to transfer cryogenics from E-4 to the cryogenic feedcan in E-4R-Center but are not installed. A cryogenic expansion box must be modified from an existing p-bar expansion box.

6.6 Power Requirements

As described in Section 4.5, this experiment requires that the magnets operate with a high ramp rate (100 A/s) and continuous cyclic operations between 1000 A and 6000 A. Available

at the E-4R pole building is the Main Injector prototype power supply which will remain in an operating condition. The operation of the two SSC dipole magnet system requires 6000 A at 40 V. The E-4R facility, which has operated reliably for several years, can provide a maximum of 9500 A at 1000 V. Power is not connected to the magnets at the present time. When approved, water cooled conductors will be used to connect the power supply to the magnet system. It appears that the existing power supply control system is adequate to provide the phase locked current wave form and other controls required for this experiment.

7. IMPORTANT SYSTEMATIC EFFECTS AND THEIR MITIGATION

In Section 3.7, the shot-noise limited performance of the system is calculated. This is the expected precision of the experiment. However, systematic effects could limit the accuracy achievable in the measurements. In this section we analyze the two most important systematic effects, the residual gas and seismic effects, their contribution to the system noise, and possible means of mitigation.

7.1 Effects of residual gas

7.1.1. Cotton-Mouton effect

In a strong magnetic field, isotropic substances show a birefringence when light is propagated through them in a direction perpendicular to the magnetic field. This phenomenon is known as the Cotton-Mouton (CM) effect [1]. Experimentally, it is found that the difference in the index of refraction for light polarized parallel and perpendicular to the magnetic field direction is:

$$\Delta n \equiv n_{\parallel} - n_{\perp} = C\lambda B^2 \qquad (7.1)$$

where C is the CM constant, λ is the wavelength of light, and B is the magnetic field. The birefringence signal from the CM effect is indistinguishable from the desired QED and possible axion signals. The SSC magnets have a cold bore at 4.35 K, so that all gases except He and H_2 will be cryopumped away. For gases with spherical symmetry such as helium, $C\lambda$ depends only on gas density ρ. For diatomic molecules such as H_2, $C\lambda$ depends as ρ/T, where T is the absolute temperature. The 1/T dependence is due to the thermal agitation of the partially aligned induced dipoles. Experimentally measured values for the Cotton-Mouton constant using 514.5 nm light at 0°C and 1 atm are: $C(H_2) = (1.61\pm0.11)\times10^{-18}\,G^{-2}cm^{-1}$ [1] and $C(He) = (3.5\pm0.7)\times10^{-20}\,G^{-2}cm^{-1}$ [2].

The Δn contribution from the CM effect must be kept below the projected experimental shot noise limited sensitivity. Thus we need to evaluate the density limits allowed for He and H_2 in the beam pipe. For the shot-noise limited 0.5 % QED experiment, $\Delta n = 7\times10^{-25}$ for an

effective B^2 of 35 T^2. Converting the CM constants to 4 K, and using a wavelength of 532 nm, the allowed densities are $\rho(H_2) < 1\times10^6$ cm^{-3} and $\rho(He) < 2.8\times10^9$ cm^{-3}. The corresponding partial pressures are 4×10^{-13} torr for H_2 and 1.2×10^{-8} torr for He. Both pressure values are at 4 K. Measurements at CEBAF [3] showed that the residual gas density in a 4.2 K magnet beam tube was less than 10^6 molecules/cm^3. The He does not present a problem unless there is a leak. On the other hand, H_2 is continuously generated in the vacuum system. One source is from outgassing of the stainless steel surfaces in the room-temperature vacuum optical chambers, and the other is from photodesorption as scattered laser light strikes the wall of the cold magnet bore. The photodesorption of hydrogen and its mitigation will be discussed in Sec. 7.1.3.

Outgassing of H_2 from the room temperature walls can be mitigated by maintaining an ultra high vacuum, $\leq 5 \times 10^{-11}$ torr, in the differentially pumped region adjacent to the cold beam tube. This pressure is within the capability of current UHV technology using Ti sublimation pumps. These will be placed immediately at the two ends of the magnet string to shield the cold bore from the H_2 generated in the warm region. Differential pumping between the magnet beam tube and the optics chambers will allow the pressure in the optics chambers to be in the 10^{-7} torr domain.

7.1.2. Faraday effect

When linearly polarized light propagates through a material in the presence of a magnetic field, there is a rotation of the plane of polarization when the magnetic field has a component along the light propagation direction. This effect is known as the Faraday effect. The angle of rotation of the polarization is given by

$$\epsilon = VlB \qquad (7.2)$$

where V is the Verdet constant of the material, l is the length and B is the magnetic field. The Faraday effect will affect the search for pseudoscalar particles but not the QED measurements. Again we will consider H_2 in the cold bore of the magnet. The Verdet constant depends linearly on the gas density. At 0°C and 1 atm, the Verdet constant for H_2 with 578 nm light is $(6.2\pm0.9)\times10^{-6}$ min/cm-G [9]. For an H_2 density of 10^6 molecules/cm^3, the Verdet constant is 6.7×10^{-23} rad/m-G. Therefore the longitudinal B field component in the magnet beam tube can

be as high as 7 T before the Faraday rotation reach the limit of 1.5×10^{-16} rad per single pass. We conclude that the Faraday effect of the residual gas is totally negligible in the present experiment.

7.1.3 Photodesorption of H_2

The photodesorption of H_2 is a concern for the present experiment and also for the next generation of large accelerators, where significant intensities of synchrotron radiation will be present in the cold beam tube of superconducting magnets. Photodesorption studies of cold beam tube were carried out for the SSC at a synchrotron radiation critical energy of 284 eV [4]. Room temperature studies were performed at CERN for synchrotron radiation having critical energies from 12.4 eV to 284 eV [5]. The CERN study showed that for a baked stainless steel tube at room temperature, the photodesorption yield of H_2 stayed constant below 63.5 eV. No data are available below 12.4 eV or at low temperatures. Although the photon energy is only 2.33 eV in our experiment, photodesorption effect is likely to be important and cannot be neglected.

As an order of magnitude estimate of this problem, we use the measured results and the model calculation of Ref. 4 for 284 eV photons in a 4.2 K beam tube. The H_2 density versus photon exposure is shown in Fig. 7.1a for photodesorbed H_2 with an average velocity corresponding to 4 K, and in Fig. 7.1b for average velocity corresponding to room temperature. (There is some evidence in Ref. 4 that H_2 may come off the surface with room temperature velocity.) These different velocities have quite different consequences for the vacuum requirement.

For case (a), the photodesorption of physisorbed H_2 (component (2) in Fig. 7.1) will be the dominant contributing factor. If the H_2 density is to be $< 1\times10^6$ /cm^3, the total exposure allowed is $\sim 5\times10^{17}$ photons/m for the Cotton-Mouton effect to become detrimental. When the Fabry-Perot cavity is in resonance, the total amount of scattered laser light per mirror for a 1 kW intracavity circulating power and 15 ppm loss on each mirror is 4×10^{16} photons/s. Most of them will be scattered into small angles. Using the interferometer geometry, we estimate that the beam tube will intercept approximately 14% of the scattered light. If this power is absorbed uniformly throughout the 30 m magnet beam tube, the photon flux from scattering by both mirrors is 3.7×10^{14} photons/s/m. This results in a run time of 22 minutes before the H_2 density becomes intolerable for a 0.5% QED experiment. It will be necessary to block the laser beam and wait

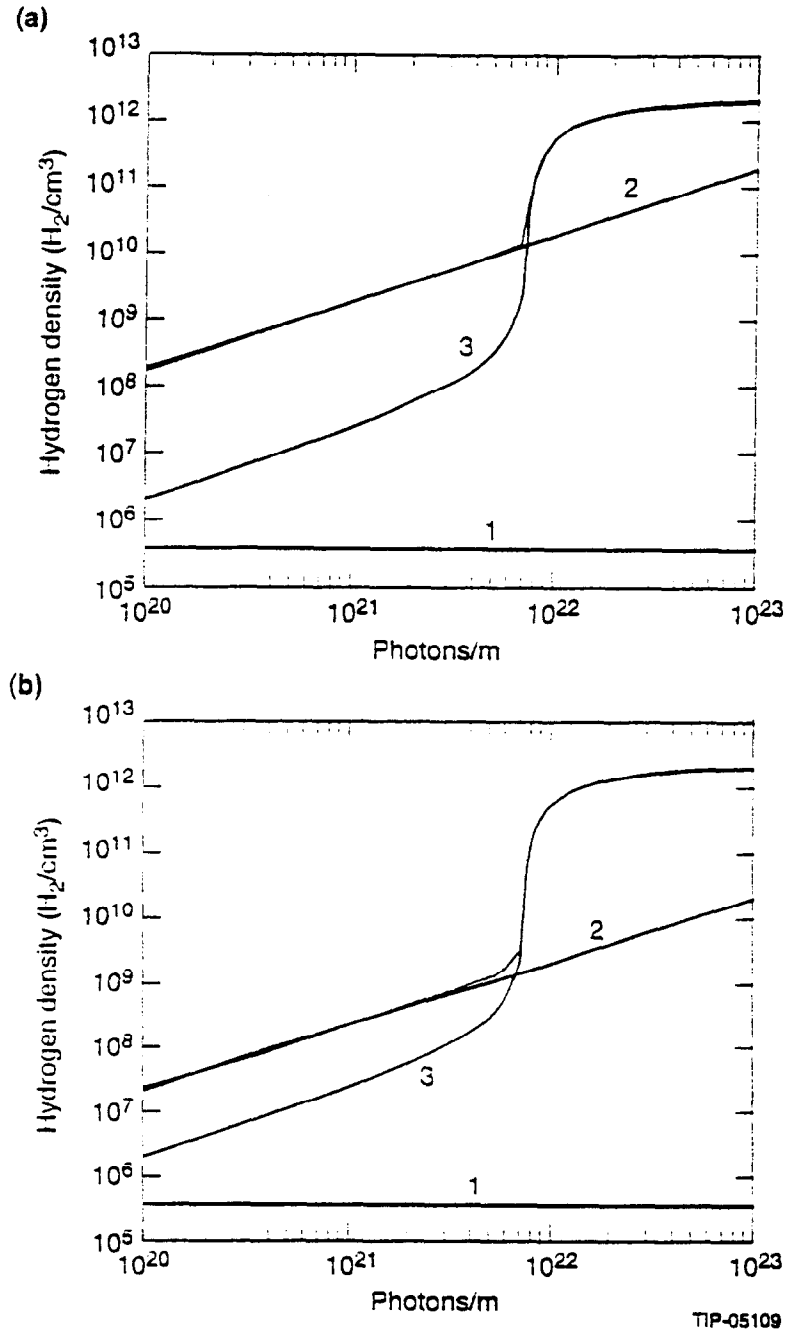

FIG. 7.1 Model calculations of H_2 density versus photon exposure in a cryosorbing beam tube; (a) $v = 2.1 \times 10^4$ cm/s and (b) $v = 1.8 \times 10^5$ cm/s. The three density components shown are (1) photodesorption of tightly bound H_2, (2) photodesorption of physisorbed H_2 and (3) the H_2 isotherm. From Ref. 4

for the H_2 to be pumped out. Solutions to mitigate the photodesorption of hydrogen in the cold beam tube will be described shortly.

Now consider the case of Fig. 7.1b, in which the photodesorbed H_2 moves with room temperature thermal velocity. Since the mean free path is much larger than the diameter of the beam tube, these "hot" H_2 molecules may contribute to the CM effect as if they are at room temperature. Extrapolating Fig. 7.1(b) to the allowable density value of 7×10^7 /cm^3 at 300 K, the run time is increased to 11 days.

Because the two results are so vastly different in their impact to the experiment, the velocity distribution of photodesorbed H_2 by 2.3 eV laser light should be measured. Laser spectroscopic techniques, such as two photon or Raman spectroscopy, can be used to measure the velocity distribution unambiguously. It is also possible to probe the density of the H_2 inside a 4.2 K beam tube using a hydrogen ion beam method [6]. Depending on the results of photodesortion studies, the H_2 density may be reduced with the following methods:

1. A Ti sublimation pumping system may be installed in the inter-connect region between the dipole magnets to help pump out some of the desorbed hydrogen. Another motivation for putting in an additional pumping section in between the magnets is that it will help to reduce scattered light by providing a place for the scattered light to be absorbed.

2. Design baffles and light traps so that the scattered light is absorbed in the interconnect pumping regions or in the end feed can region where the magnetic field is low. Pumps will be used to straddle these regions to prevent H_2 from diffusing into the cold bore regions.

3. Use a coaxial perforated tube as a liner in the cold beam tube [7]. The physisorbed molecules would accumulate behind the liner and stay out of view of the photons. A liner can be designed with a sufficient number of holes to ensure that the equilibrium H_2 density is kept below 10^6 /cm^3. A partial liner could be formed using sections of high purity graphite which also serve as a distributed light absorber and in-situ cryopump of H_2. The surface morphology of the liner could be shaped (for example, by grooving) to reduce phase noise due to scattered light. This is important for reducing the seismic motion contribution to the birefringence signal. See Section 7.2.

4. The beam tubes of the prototype SSC magnets were not heat-treated or coated. A combination of N_2 glow discharge and 90% Ar + 10% O_2 glow discharge could be run along the

magnet beam tube to clean the surface of the stainless steel. Studies indicate that this combination appears to be the most effective method in reducing photodesorption [8].

The implementation of the steps above should allow the run time between experimental interruptions to reach a more reasonable level. Note that photodesorption is only important when the Fabry-Perot cavity is actually in resonance and the intracavity laser power is high. It is not important during most of the testing and setup studies.

7.2 Effect of Seismic Motion on Scattered Light

Light hitting a mirror may be scattered out of the main beam of the interferometer. This scattered beam may in turn make its way back into the main beam by reflection or scattering off the walls and baffles of the surrounding beam pipes. The scattered beams travel a different path length relative to the main beam and contribute a phase shift to the main beam signal. The scattering phase shift changes as the beam pipe is moved from seismic effects and acoustic perturbations. Thus the scattered light contributes a phase noise which,without mitigation, would severely degrade the system performance of the interferometer.

The scattered light problem of the proposed interferometer is similar to that encountered in the laser interferometer for gravitational wave detection (LIGO project [10]). Methods developed for the LIGO and GEO projects will be used here to obtain an estimate of the effect [11,12]. However, the proposed interferometer has additional electro-mechanical effects. The magnets will change length and flex, in phase with the ramping of the magnetic field. For a complete analysis we also must keep track of the phase evolution of the two orthogonal polarizations.

7.2.1. Reflection from Pipe Walls

One improtant process for noise generation in the experiment is the recombination of scattered or diffracted light into the main beam mode. For example, light scattered from a mirror travels down the pipe, reflects at least once off the pipe walls, reaches the other mirror, and scatters back into the main beam. Since the reflectivity of the pipe walls are large only at grazing angles of incidence, baffles are used to block the small angles and force the light-beam to reflect at large light-beam pipe angles. In general the light will then have to undergo many

reflections as it travels from one end of the pipe to the other. The larger the number of reflections, the more likely the light will be scattered away and be absorbed by the walls of the beam tube.

Ideally the walls and baffles should be blackened to lower the reflectivity and increase light absorption. The beam tube of the SSC magnets is made of unpolished stainless steel. One solution to decrease the reflectivity is to introduce a liner or sleeve into the tube. The material and surface topology of the liner would be chosen so that the liner becomes a distributed light absorber throughout the bore. The liner also serves to reduce the photodesorption of H_2 in the cold bore - a topic that is important for the Cotton-Mouton effect discussed in Section 7.1.

7.2.2. Motion of Beam Tube

An unavoidable source of vibration for the beam pipe is ground motion. The amount of seismic motion is site dependent and time dependent. In general, the most quiet sites are deep underground and free of mechanical equipment and personnel. The E4-R area at Fermilab for this experiment is at ground level and somewhat isolated from mechanical equipment. The site is quietest at night. Fig. 7.2 shows the spectral density of the vertical seismic displacements measured at the E-4R magnet tunnel under quiet conditions [13]. At frequencies above 15 Hz, the vertical displacement has an approximately $1/f^2$ dependence, except for resonances at harmonics of 10 Hz and 15 Hz. The displacement is somewhat level between 1 Hz - 10 Hz, and increases below 0.4 Hz due to the microseismic peak around 0.2 Hz. At 1 Hz, the vertical motion is ~ 7×10^{-9} m/$\sqrt{\text{Hz}}$. The character of the vertical displacement spectrum at E4-R is fairly typical of other laboratories [14], e.g., see Fig. 7.3. The horizontal motion at E4-R is very similar to the vertical motion, except the Q of the resonances is somewhat larger.

Analysis from LIGO shows that the phase noise is mainly due to the back scattering from the first set of baffles [11]. The sensitivity limit due to beam tube motion is expressed in terms of the square root of the spectral density of noise h(f), in units of "strain per root Hz". For our experiment, h(f) = $\Delta L/L$ = $\Delta n/n$, and is given by [15]

$$h(f) \approx \sqrt{4\pi\alpha^2\beta \ln\left(\frac{l_1}{l_2}\right)}\,\frac{\lambda}{R}A(f)\,\frac{\xi(f)}{L} \qquad (7.3)$$

In the above equation, it is assumed that the scattering probability of main-beam light

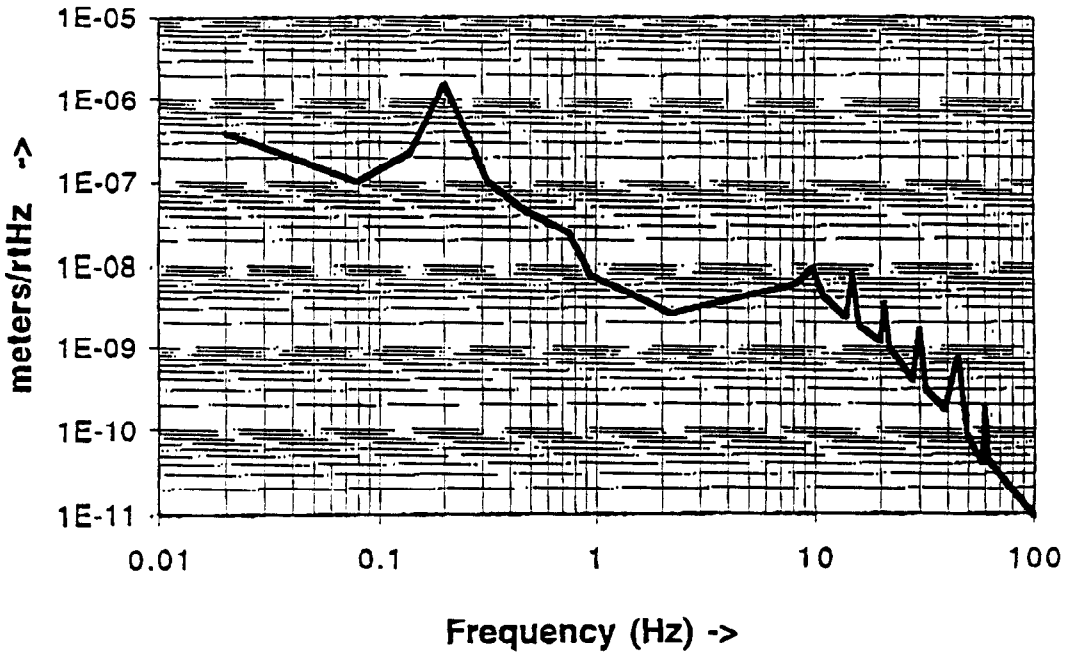

FIG. 7.2 Measured spectral density of vertical vibrations at the Fermilab E-4R magnet tunnel.

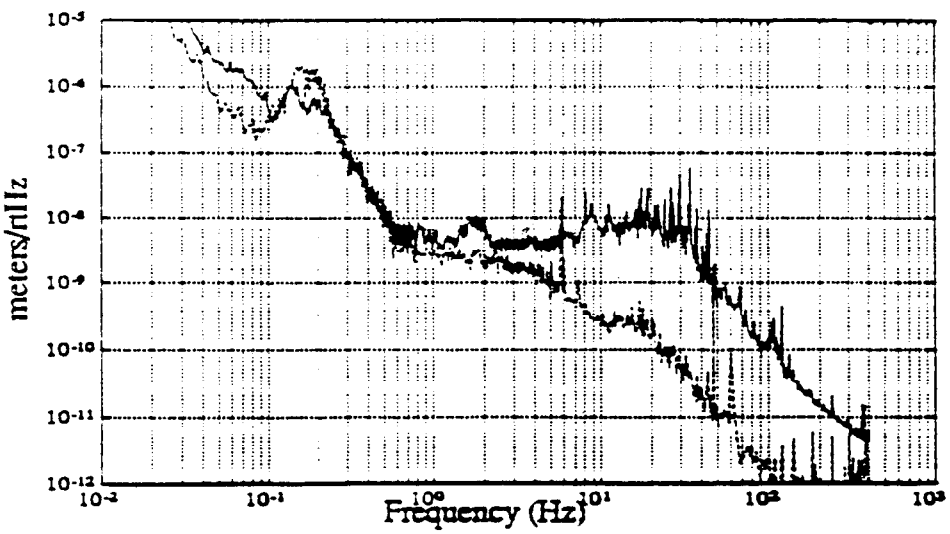

Figure 7.3 Measured spectral density of amplitude of vertical seismic motion. Upper curve is lab # B042 of JILA at the Univ. of Colorado, Boulder. Lower curve is Building 8 of NIST, Boulder, which is considered to be a "quiet site".

from an interferometer mirror into unit solid angle around a direction that makes an angle θ with the normal of the mirror follows the form $dP/d\Omega = \alpha/\theta^2$. For our interferometer geometry and a 15 ppm loss mirror, $\alpha \approx 2.4\times10^{-7}$. L is the length of the cavity (50 m), l_1 and l_2 are the distances from the mirror to the furtherest and closest sets of baffles (45 m and 5 m), respectively. λ is the wavelength (532 nm), and R is the beam tube radius (2 cm). β is the back scatter probability from the baffles and is ~ 10^{-2} for most materials. $\xi(f)$ is the square root of the spectral density of seismic displacements of a typical point on a typical baffle, and A(f) accounts for amplication of the seismic motion due to excitation of beam tube normal modes. For an estimate we will assume that the beam pipe and baffles are sufficiently well-anchored so that $A(f)\xi(f)$, ~10^{-8} m /$\sqrt{}$Hz, on the order of the seismic noise. The noise contribution to the sensitivity of the interferometer is $\Delta n/n \approx 7 \times 10^{-22}$ /$\sqrt{}$Hz. The motion contributes a noise that is approximately 1.5 times the shot-noise limit of the proposed interferometer. Thus seismic effects will be detrimental to the sensitivity of the proposed experiment.

The above calculation is based on the amplitude of the seismic disturbace at one point. However, at the low frequency of modulation (~1Hz) of this experiment, the wavelength of the seismic disturbances are on the order of kilometers, and is substantially larger than the length of the interferometer. As shown in Fig. 5 of Ref. 13, the vertical seismic motion at E4-R is coherent over the length of the interferometer for frequencies between 0.09 Hz and 1 Hz. Due to the common mode motion of the apparatus, the seismic effect calculated above could be less by a factor of 10 [16], and contributes at about 20% of the shot noise limit of the experiment.

7.2.3. Recommendations Regarding Scattering

The calculations above show that scattered light may not be negligible for the proposed experiment. Carefully designed baffles are needed to suppress as much as possible the scattered light from recombining into the main beam mode. The small diameter of the SSC magnet beam tube does not allow baffles with optimal height for stray light suppression. However, a baffle height of 0.9 cm can be used without introducing diffraction losses that are comparable to the mirror losses into the Gaussian beam mode of the propagating laser. As a first design, the first set of baffles would be placed at a distance of 5 m from the mirrors. Ideally, subsequent baffles should be placed at the anchor point of each magnet. This is to ensure that the motion of the

baffles is controlled by the ground alone, and not by other effects such as ramping of the magnetic field. Again this may not be possible. The use of a liner as a distributed light scatterer/absorber looks promising and warrants serious consideration.

The above calculations are at best a rough estimate of what the scattering noise may be. We have not included the scattering due to the flexure motion of the interferometer, and we have ignored the different scattering probability of the two polarizations. A numerical analysis of the stray light problems, using programs such as APART and GUERAP, could be employed to determine the phase noise that will be introduced due to ground or other motions. These Monte-Carlo programs will also allow for optimization of baffle or liner and light trap placements/configurations. As input to the numerical simulations, it will be necessary to know the amount of ground motion at the experimental site, the effect of magnet ramping, and the bidirectional scattering functions of the beam pipe and possible liner/light trap materials.

7.3 References

[1]. F. Scuri, *et al.*, J. Chem. Phys. **85**, 1789 (1986).

[2]. R. Cameron, *et al.*, Phys. Lett. A **157**, 125 (1991).

[3]. William Turner, private communication.

[4]. V. Anashin *et al.*, "Cold beam tube photodesorption and related experiments for the SSCL 20 TeV proton collider", SSCL Preprint-533, (March, 1994).

[5]. J. Gómez-Goñi, O. Gröbner and A. G. Mathewson, "Comparison of photodesorption yields using synchrotron radiation of low critical energies for stainless steel, copper and electrodeposited copper surfaces", to be published.

[6]. W. C. Turner, private communication.

[7]. W. C. Turner, "Dynamic vacuum in the beam tube of the SSCL collider - cold beam tube and liner options", SSCL-preprint-404, (May 1993).

[8]. T. Kobari and H. J. Halama, J. Vac. Sci. Tech. **5**, 2355 (1987).

[9]. *American Institute of Physics Handbook,* ed. Dwight E. Gray (McGraw Hill, 1957), page 6-91.

[10]. A. Abramovici *et al.*, Science **256**, 325 (1992). A. Gillespie and F. Raab, Phys. Lett. A **178**, 357 (1993). The LIGO web site at www.ligo.caltech.edu.

[11] Eanna E. Flanagan and Kip. S. Thorn, "Scattered-light noise for LIGO", LIGO technical report LIGO-T950102-00-E, April, 1995, and references cited therein.

[12]. The GEO web site at www.geo600.uni-hannover.de/geo600/site/baffles.html.

[13]. B. Baklakov, *et al.*, "Seismic studies for Fermilab future collider projects", FERMILAB-Conf-97/383 (Nov. 1997), to be published in Proceedings of the 5th International Workshop on Accelerator Alignment, Argonne National Laboratory, Argonne, IL, October 14-17, 1997.

[14]. David B. Newell, "Six degree of freedom active vibration isolation at 1 Hz and above", Ph. D. thesis, Univ. of Colorado, Boulder (1994).

[15]. Eanna E. Flanagan and Kip. S. Thorn, "Light scattering and baffle configuration for LIGO", Report prepared for LIGO baffle review, 6&7 January, 1995.

[16]. Peter Bender, private communications.

8. EXPERIMENTAL PROGRESS TO DATE

This chapter describes the work that has been done by the collaboration over the past three years.

8.1 Birefringence Measurement (JILA/NIST)

At JILA, a preliminary investigation of measuring small phase differences with frequency technique was carried out with a 27.7 cm fixed-length Fabry-Perot cavity having a finesse of 4.5 $\times 10^4$. The laser was a frequency stabilized He-Ne laser, and the transmitted beam of the Fabry-Perot cavity was used for locking. The optical frequency of the laser was servo-controlled to bring the vertical polarization component to be in resonance with the cavity. The frequency of the horizontal polarization component was brought into precise resonance with the next cavity order by shifting with an acousto-optic modulator. For this study, the seismic contribution was not common mode and remained an important noise source. A rotating half-wave plate was placed in front of the cavity to modulate the two polarization directions in the cavity. The beat frequency between the two polarization components were recorded as a function of the half-wave plate angle. No magnetic field was applied. The recorded change in the beat frequency is shown in Fig. 8.1(a). The data show a sinusoidally varying phase changes as the polarization of the incoming light is being rotated, indicating that there is a birefringent direction in the cavity. This effect is due to the birefringence of the mirror coating. The 304 Hz frequency difference between the two polarization resonances corresponds to a mirror induced phase difference of ~3.4 μrad per pass.

The laser power was < 20 μW for each polarization. The Fourier distribution of the measured birefringence is shown in Fig. 8.1 (b) for frequencies near the proposed magnet modulation frequency (5 mHz). The sensitivity is about -80 dB relative to the mirror birefringence of 304 Hz, giving an index of refraction measurement sensitivity $\Delta n/n$ of 6.5×10^{-17}. These first data have a noise level that are many times above the shot noise limit. The noise is due to problems of inadequate optical isolation and seismic isolation, and excessive acoustic noise in our laboratory. Another important noise source is from the dynamic mirror birefringence which is dependent on the light power and polarization. It was found that with linearly polarized light, the polarization interaction gave rise to a birefringence of 0.6 μrad/W. For circularly polarized light, there was no detectable birefringence. These light power dependent dynamic

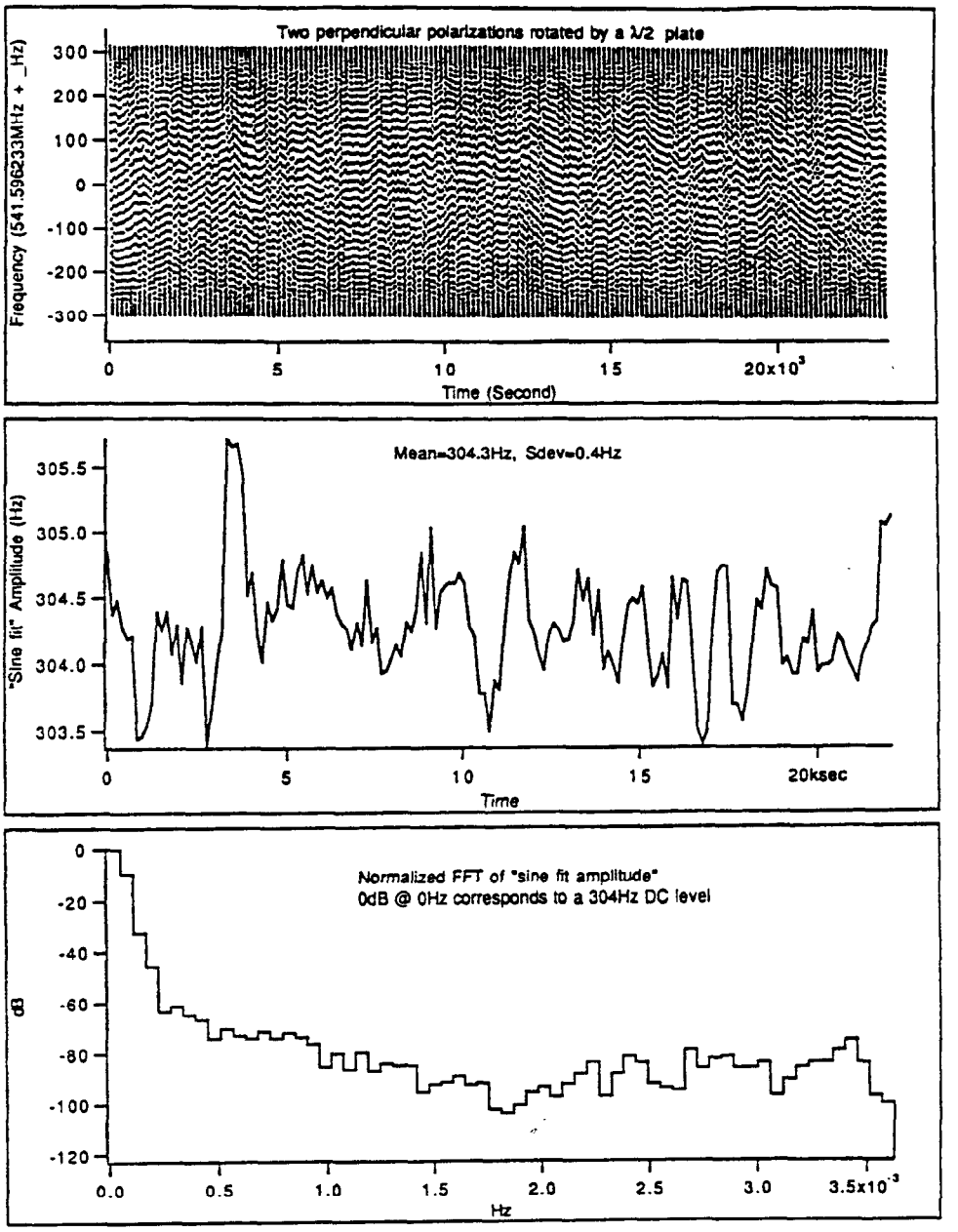

FIG 8.1 Birefringence data measured with preliminary spectrometer. (a) Time series showing 160 cycles of sinusoidal frequency change between two different cavity modes, as the input linear polarization was rotated relative to the cavity birefringence axes.
(b) Amplitude of sinusoid fit to data. Plotted data are fitted cycle-by-cycle, and averaged over four cycles, corresponding to a full 360° rotation of the half-wave plate.
(c) Fourier distribution of measured birefringence. Near our projected magnet modulation frequency, the present sensitivity is about -80 dB relative to the mirror birefringence and is limited by a number of remediable systematic effects.

effects are under active investigation in our collaboration.

8.2 Development of the 2 m Vacuum Fabry-Perot Interferometer (CSU)

A 2 m vacuum Fabry-Perot interferometer was constructed at CSU. The finesse of the cavity, ~1000, is sufficient for testing the mirror birefringence effect. A simple lead/rubber stack is used to isolate the mirrors from ground vibrations. The two mirrors of the Fabry-Perot are not rigidly tied together as in the JILA fixed length interferometer, in order to better simulate the conditions for the 50 m interferometer.

A commercial frequency-doubled Nd:YAG laser at 532 nm (Lightwave Electronics Model 142) is used as the light source. The laser provides good output power, >150 mW, but has large frequency drifts and noises. The frequency control of the laser is insufficient for the current experiment. We have developed a specific feedback control scheme for this commercial laser to stabilize its frequency, by using laser saturated absorption to lock the laser on a hyperfine transition of the P(132) 36-0 transition in I_2 (line #1103 of the iodine atlas [1]). The laser linewidth is reduced from its 1 MHz free run stability to less than 10 Hz (in a 1 sec measurement time). The stability of the laser enables us to lock the Fabry-Perot cavity resonance to the laser without much difficulty, and investigation of the laser power influence of mirror birefringence is under way. A set of cavity servo electronics was also constructed for use at Fermilab.

8.3 Progress at Fermilab

The Fermilab SSC magnet string test facility at E4-R has been modified to accommodate this experiment. This facility is a tunnel at ground level 120 m long extending south from the E4-R pole building. A magnet power supply and source of cryogenics are already available in the pole building. The magnet tunnel, which was being rebuilt because of interference with the Main Injector construction, was modified to include two rooms (Center Hall and South Hall) for the interferometer end stations. Subsequently, two SSC magnets were installed in the South tunnel supported by the SSC low profile magnet test stand. The SSC cryogenic feed-can and turn-around can were installed in the Center and South Hall, respectively. The magnets have been aligned, and a clear beam tube aperture of 38 mm has been achieved. To remove water vapor accumulated on the super insulation in the insulating vacuum system, the entire magnet system is maintained under vacuum for six months and are currently being purged with dry

nitrogen. Optical tables with clean air systems have been installed in the Center and South Halls. A prototype seismic vibration isolation system for supporting an interferometer mirror has been installed in the South Hall. A prototype digital control and monitoring system to provide interferometer mirror active vibration isolation and positional control is installed.

8.3.1 Laser System

An early model of the commercial Lightwave 142 laser (532 nm) was purchased in 1996 for Fabry-Perot interferometer related R&D. However, this laser steadily lost power, became unstable and eventually failed. It proved to be too expensive to repair. For the frequency stability we require, the collaboration decided that it would be best to use an infrared Nd:YAG laser, Lightwave 126 at 1064 nm, and do the frequency-doubling ourselves. The laser is currently installed at the E-4R South Hall. The development of a bow-tie ring cavity for frequency doubling with a $MgO:LiNbO_3$ crystal using the Hansch-Couillaud locking scheme [2] is underway.

A temperature stabilized, fixed length, 30 cm Fabry-Perot interferometer has been developed for short term laser frequency stabilization [3] using the Pound-Drever-Hall locking technique [4]. The acousto-optic and electro-optic modulators, detectors and electronics have been tested, but final system performance awaits completion of the frequency doubling.

The laser presently being used in the development of the seismic isolation systems is an air cooled Ar ion laser. This laser has the advantage of operating at low power, thus enhancing personnel safety during the early stages of this study. A preliminary laser safety interlock system is installed for the E4-R experimental area.

8.3.2 Seismic Vibration Isolation System

Our present line of development of the passive seismic vibration isolation system [4] for the interferometer mirrors is described in Sections 3.4 and 5.2. A schematic layout of a vibration isolation tower is given in Fig. 5.1. The tower rests on a concrete slab which is isolated from the general floor of the hall by 25 cm of sand. This provides the first level of passive isolation. An inverted pendulum [6] which acts as a low pass filter provides the horizontal isolation while a torsion-crank type system [7] provides vertical isolation. A long double pendulum gives a very soft suspension. Mirror damping and orientation are controlled by action-at-a-distance sensors

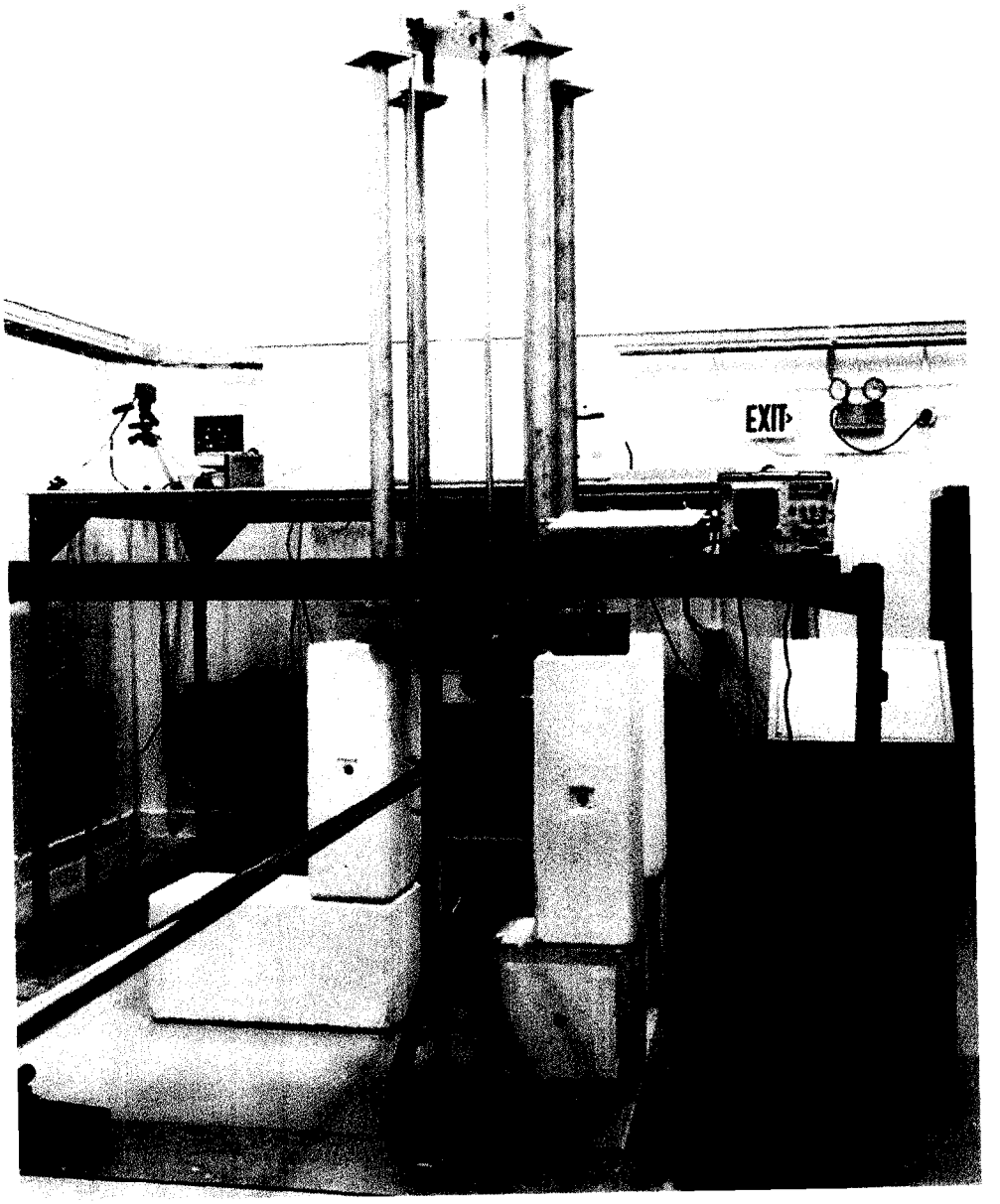

FIG. 8.2 An inverted pendulum for vibration isolation is under development at the South Hall of E4-R.

and pushers [8] acting on the upper mass of the double pendulum.

A two meter inverted pendulum was designed [9] to have a resonant transverse frequency of 30 mHz when supporting a load of 136 kg. Fig. 8.2 shows the inverted pendulum set up in the E4-R South Hall. The three pendulum legs, each 2.5 cm in diameter, were evenly spaced on an 18 inch diameter circle. To raise the violin modes of the legs above our region of interest, they were made of thin wall stainless tube. The pendulum leg "hinges" have 8.1 mm diameter neck regions at each end of the tubes. The assembled system had a measured transverse resonance frequency of 38 mHz with a supported load of 102 kg. The measured torsional frequency was 2.5 Hz.

The originally proposed torsion-crank suspension was studied theoretically and explored for instabilities. A simple low-Q prototype was constructed and demonstrated a vertical resonant frequency of 200 mHz [10]. The expected equilibrium instabilities were also observed. A new design is underway.

8.3.3 Active Vibration Dampening, and Mirror Positioning and Pointing System

The active dampening and positioning system consists of LED shadow detectors (sensors) which sense the relative motion of the inverted pendulum top plate and marionette, and electromagnetic coils (pushers) which act at a distance through constant gradient fields to push permanent magnets attached to the inverted pendulum top plate and to the marionette [11]. A prototype of this system, consisting of two sensors and two pushers, has been implemented to sense and dampen azimuthal motion of the marionette. Using the control system described below, early tests give an angular stabilization of the marionette supported interferometer mirror of 60 μrad. The actual mirror angular stabilization should be considerably better than 60 μrad because the measuring technique also includes the angular deviations from laser pointing instability.

8.3.4 Digital Feedback, Control and Monitoring System

A control and monitoring system has been developed using techniques adopted from the Fermilab Tevatron and Main Injector control systems [12]. For many feedback functions the input signals come from one hall while the controlled device is in the other hall; this led to the installation of the distributed control system shown in Figure 8.3. A VME crate containing CPU,

ADC and DAC cards is located in each hall. The CPUs are connected by an optical fiber link using a Reflective Memory Module; inputs known to one CPU are therefore also known to the other CPU. Each VME CPU, using all the input signals, calculates and controls only the pushers (and PZT's) which are located in its hall. The VME data collection and processing is monitored via EtherNET on a remote computers using Labview. The constants for data processing and feedback control are down loaded from remote computers using Labview and Remote Procedure Calls to the VME CPU. This system has been in operation for six months and operates well. All feedback and control studies use this system exclusively.

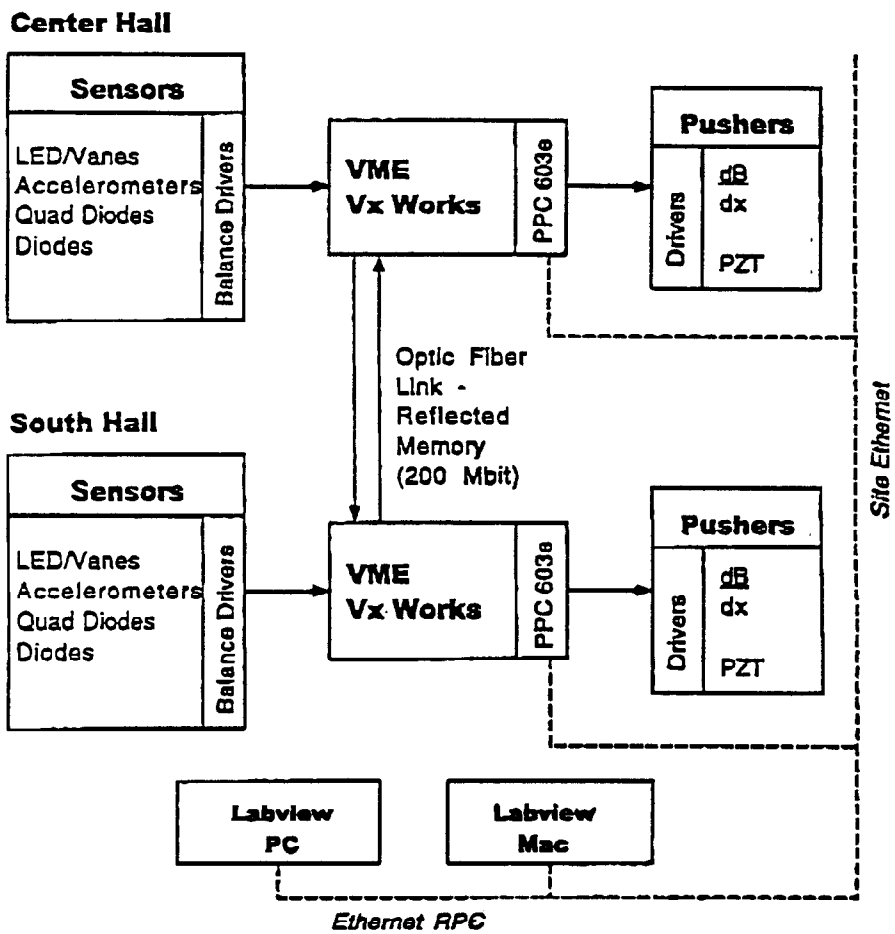

FIG. 8.3. Overview of the Digital Control and Monitoring System. A VME computer based system operates at each end of the interferometer, i.e., in the Center Hall and the South Hall. By use of reflected memory, the sensor inputs are shared between the two computer memories. These systems are monitored and controlled using Labview programs operated from remote computers via Ethernet RPC's.

8.4 References

[1]. S. Gerstenkorn and P. Luc, "Atlas du spectre d'absorption de la molecule de l'iode entre 14800 -20000 cm^{-1}," (Editions du C.N.R.S., 15 quai Anatole-France, 75700 Paris)

[2]. T. Hansch and B. Couillaud, "Laser Frequency Stabilization by Polarization Spectroscopy of a Reflecting Reference Cavity." Opt Commun. **35**, 441 (1980).

[3]. J. Bergquist, M. Itano and D. Wineland, "Laser Stabilization to a Single Ion." Time and Frequency Division, NIST,Boulder, CO 80303.

[4]. R. W. P. Drever, J. L. Hall, *et al.*, Appl. Phys. B **31**, 97 (1983).

[5]. F. Nezrick, "Measuring the Effect of a Magnetic Field on the Speed of Light in Vacuum" to be published in proceedings of "Frontier tests of QED and physics of the vacuum." Sandansky, Bulgaria, 9-15 June 1998.

[6]. M. Hill, L. Holloway, *et al.*, "A Front End Seismic Isolation Stage for VIRGO," VIRGO Internal Report, May 20, 1994.

[7]. J. Winterflood and D. Blair, "A long-period vertical vibration isolator for gravitational wave detection," Submitted to Phys. Letts. A, February, 1998.

[8]. J. Winterflood, *et al.*, Rev. Sci. Instrum. **66**, 2763 (1995).

[9]. Peter Fisher, "Inverted Pendulum Vibration Stabilization for 50 m Interferometer at E4R," Fermilab Internal Note 877-17, August 29, 1997

[10]. F. Nezrick, "Prototype Torsion-Crank Vertical Isolator," Fermilab Internal Note in Preparation 877-34, June 28, 1998

[11]. F. Nezrick, "Preliminary Concepts for Interferometer Mirror Control System," Fermilab Internal Note 877-15, September 17, 1997

[12]. J. Marler and F. Nezrick, "Interferometer Digital Feedback and Control System," Fermilab Internal Note 877-23, January 20, 1998

9. SCHEDULE OF EXPERIMENT

9.1 Introduction

The proposed duration of this project is five years divided into two discrete phases. Phase I, the first three years of the experiment, will have efforts under way at Colorado and at Fermilab. In Colorado, a 2 m high-finesse Fabry-Perot interferometer will be constructed and used as a testbed to perfect the two mode interferometer locking technique and digital birefringence measuring scheme and to study systematic birefringence effects of dielectric mirrors. At Fermilab the existing experimental area at E-4R will be utilized to develop a prototype seismic vibration isolation system for the interferometer mirror supports, a digital feedback control system to position and align the interferometer mirrors, a laser system for initial interferometer use, and a low finesse 50 m Fabry Perot Interferometer. E-4R will also be utilized to study optical baffles to suppress wall reflections in the 50 m beam pipe, getter systems for vacuum control in the interferometer beam pipe, and to make photodesorption measurements in our actual beam pipe at 532 nm. The Colorado and Fermilab systems will be merged in the third year. The goal of Phase I is to demonstrate a sensitivity of the 50 m interferometer at the QED level.

In Phase II the full integration of the work developed by the Colorado and the Fermilab groups is completed at the Fermilab experimental area. The superconducting magnet system is commissioned; power and cryogenics are supplied; the quench protection and magnet control system is installed and tested; the magnets are aligned and the beam tube is aligned. The ultra-high-vacuum systems associated with the interferometer beam tube are commissioned. The high finesse optical system with two mode locking will be commissioned in the 50 m interferometer in the fourth year and the system sensitivity and signal-to-noise ratio improved. The last year is devoted to the actual measurements of the experiment and reduction of systematic errors.

Since there is considerable experience in the laser interferometer gravitational wave projects, the accelerator community, and in our collaboration on problem such as vibration isolation, laser stabilization, cavity locking, superconducting magnet operations, scattered light, and residual gas effects, we expect the problems in these areas to be only hurdles rather than impassable barriers. The potential backgrounds in the experiment which are of greatest concern

are those which may be phase correlated with the magnet ramping. These include the Cotton-Mouton effect from photodesorbed H_2, light scattering changes associated with beam tube motion, and other sources which may not have been anticipated. A full test of these effects require the full magnet system, laser, and 50 m interferometer.

Consequently, our plan is based on a direct attack on all major problems, including the design and construction of the optical, vacuum and vibration isolation system from early in the project. The major intermediate steps are (1) an experimental study of photodesorption, (2) prototype testing of vibration isolation systems using a low finesse 50 m cavity, and (3) extensive experience with a 2 meter Fabry-Perot interferometer at Colorado State/JILA before attempting to install a full 50 m high finesse interferometer at Fermilab. Note that the 2 meter interferometer makes stringent tests of the optical, vacuum and vibration isolation systems to be used in the 50 m interferometer.

9.2 Yearly milestones

Prior to Year 1:

Commission E-4R Experimental Area

Install SSC Dipole magnets

Install Cryogenic end cans without cryogenic hookup

Operational basic lasers at CSU, NIST and Fermilab

Year 1:

Colorado

Stabilized laser operational

2 m high finesse interferometer operational

Develop two mode interferometer locking technique

Develop birefringence measurement scheme

Fermilab

Stabilized frequency doubled laser operational

Optics Vacuum Chambers fabricated and installed

Prototype Seismic vibration system developed

Develop lock/servo electronics and suspended mirror control system.

Year 2:

Colorado

Construct vacuum electro-optic birefringence spectrometer

Determine effect of laser power on birefringence of the mirrors

Fermilab

50 m low finesse interferometer assembled

Construct improved vibration isolation system

Interferometer auto laser steering and mirror alignment system

Start cryogenic photodesorption studies

Study methods to reduce scattered light in the beam tube.

Year 3:

Colorado

Test stray light, and locking of the 2 meter interferometer.

Demonstrate dynamic range and accuracy of interferometer locking technique

Determine optical noise characteristics of birefringence measurement with the 2 meter interferometer.

Fermilab

Confirm performance of passive and active seismic isolation systems.

Construct beam tube liner system

Start Merging Systems from Colorado and Fermilab

Demonstrate Sensitivity of 50 m interferometer at the QED Level.

Year 4:

Full Integration of Colorado and Fermilab systems

Install Magnet Cryogenic System

Install Magnet Power System

Install Magnet Control System

Characterize motion of magnets during ramping.

Investigate H_2 levels in the magnet bore tube and the effect of scattered light.

High finesse 50 m interferometer established

Begin initial experimental program using magnets and interferometer.

Study systematic noise sources and noise reduction techniques.

Measure initial QED signal.

Year 5:

Make precision measurement of QED effect.

Conduct axion search.

Define any future plans for experiment

10. DISTRIBUTION OF EFFORT AND COST ESTIMATES

This section represents the result of a bottom-up cost estimate of this experiment assuming a distribution of effort among the collaborators as given below. This estimate includes the basic assumptions that (1) duplication of effort within the collaboration will be minimized, (2) existing items used in the experiment will be indicated, and (3) maintenance of the non-optics part of the experiment would be provided by the Beams Division and Particle Physics Division of Fermilab.

The experiment is proposed in two phases, for a total duration of 5 years. In Phase 1 the interferometer is demonstrated to have a sensitivity at the QED level. In Phase 2 the superconducting magnets are commissioned, the interferometer sensitivity is improved and final measurements are performed. The estimated cost for each year of each phase will be presented.

10.1 Distribution of Responsibilities

10.1.1 Colorado State University & University of Colorado/JILA

In Phase 1 the Colorado group will be responsible for the development of a 2 m Fabry-Perot laser interferometer and the birefringence and rotation measurement systems, with a design goal of measuring the change in the index of refraction between two orthogonal polarizations of a beam of light with shot-noise limited sensitivity. This effort will be undertaken at these institutions under existing grants from NIST, and anticipated grants from NIST and NSF. After preliminary studies with the 2 m interferometer are complete, this optical system will be moved to Fermilab and integrated with the 50 m interferometer. In Phase 2 the Colorado group will be primarily responsible for maintaining and improving the measurement capability of the 50 m interferometer and will share in the data taking and analysis.

10.1.2 Fermi National Accelerator Laboratory

The Fermilab effort will be divided among the Beams Division and the Particle Physics Division. The Beams Division will be responsible for the experimental area at E-4R, the research and development of the active and passive vibration isolation systems, for powering and cooling the two SSC Dipole magnets, for the magnet control and safety, for the beam tube and optical

chamber vacuum systems and the beam tube light baffle system. The Particle Physics Division will be responsible for the optical vacuum chambers and support for designing and implementing the vibration isolation control system and for vacuum support in the study of photodesorption of H_2 by laser light. General operating support for the Fermilab experimental group will be requested from the BD and PPD in proportion to the related efforts in those divisions.

In Phase 1 the experimental area will become operational and a preliminary 50 m optical system will be established. Vibration studies in situ will lead to a vibration isolation system for the interferometer mirrors and magnets. Studies of photodesorption will lead to a beam tube liner and vacuum system satisfactory for the experiment. Light scattering tests and calculations will aid in the development of a beam tube light baffle system. In Phase 2 the SSC Dipole magnets will be operational and initial debugging of the full 50 m interferometer with magnetic field will begin. The Fermilab group will share in the responsibility of data taking and analysis.

10.2 Cost Estimates

The M&S costs are estimated for Fermilab and non-Fermilab contributions for Phase 1 and Phase 2 separately. The Fermilab cost reflects both Beams Division and Particle Physics Division contributions. The non-Fermilab cost is the sum of the contributions from Colorado State University and University of Colorado/JILA. Table 1 and Table 2 give the cost estimates for Phase 1 and Phase 2 respectively. The value of materials already in hand is shown in brackets. As seen from Table 1, the Fermilab M&S cost for Phase 1 years 1, 2 and 3 is \$95k, \$70k and \$56k respectively. The major expense in the first two years are the Optics Towers and the Seismic Isolation systems. The Fermilab group is requesting a Research Associate for the duration of the experiment. A half-time electrical and half- time mechanical technicians are also required. A miscellaneous operating budget of \$1.5k per month is also estimated. Note that the equipment in-hand is valued at \$ 253k. This equipment has been acquired over the past several years from the SSC liquidation, DOE-REAPS surplus, internal Fermilab surplus and Fermilab Physics Departmnet R&D support.

We propose that Phase 2 proceed only if Phase 1 is successful in reaching QED sensitivity level. As seen from Table 2, the Phase 2 Fermilab M&S costs are \$190k and \$63k for years 4 and 5 respectively. Again a miscellaneous operating budget of \$1.5k per month is estimated.

The value of the additional equipment needed for Phase 2 which is already in-hand amounts to $1,585 K. The surplus sources have been good to us.

10.3 Funding Options for the Colorado State/Colorado Universities

The group at Colorado State University is supported by a NIST Precision Measurements Grant, which carries an award of $50 K per year for three years, for a total of $150 K. This grant has allowed us to purchase equipment to set up the laser source, laser stabilization, preliminary birefringence spectrometer, and the 2 m vacuum Fabry-Perot interferometer. The equipment in-hand is valued at $90K. This is shown in brackets in Table 1. The grant also pays for CSU Graduate Research Assistants. Anthony Glueck was at Fermilab, working in the E-4R experimental area. Shannon Siefken and Shie-Chang Jeng are at Colorado State University, working on the 2 m interferometer. The group at JILA/Univ. of Colorado is supported by existing programs in the Quantum Physics Division of the National Institute of Standards and Technology.

The Colorado groups plans to submit a proposal to the National Science Foundation, requesting $300K to support personnel, travel and further experimental development costs by CSU and CU/JILA. The M&S costs are listed in Tables 1 and 2. A previous proposal to NSF was favorably reviewed for its physics and methodology. However, a main concern of the reviewers was that the project was not officially approved by Fermilab, and the proposal was rejected. Thus, approval of the proposed experiment by Fermilab will be crucial in order for the Colorado groups to obtain funding from agencies such as the National Science Foundation.

M&S Cost Estimate for P-877 Phase 1

	Element	Fermilab	CSU/JILA
		k$	k$
1.0	2-meter Interferometer		50+(67)
1.1	Laser		(23)
1.2	Optics & mounts		25+(7)
1.3	Electronics		15+(10)
1.4	Vacuum System		10+(10)
1.5	Optical table		(14)
1.6	Vibration Isolation System		(3)
2.0	Two frequency cavity locking system		68+(13)
2.1	Optics		40+(10)
2.2	Electronics		28 + (3)
3.0	50-meter Interferometer-laser and optics	35+(135)	(10)
3.1	Laser	(30)	
3.2	Frequency Doubler	5+ (5)	(5)
3.3	Laser frequency stabilizer	10+(15)	(5)
3.4	Optics	20+(10)	
3.5	Optical tables	(25)	
3.6	Class 10 enclosures	(50)	
4.0	50-meter Interferometer-vacuum system	80+(66)	
4.1	50-m test beam tube & stands	(4)	
4.2	Optics Towers (Center & South)	70+ (2)	
4.2	Vacuum system	10+(60)	
5.0	50-meter Interferometer-seismic isolation	94+(13)	
5.1	Vacuum feedthru & base support	20	
5.2	Inverted Pendula	25+(6)	
5.3	Torsion Crank Pendula	20	
5.4	Marionette & Mirror Bob	15+(3)	
5.5	Electromagnetic Pushers	4+(2)	
5.6	Laser position sensors	5+(1)	
5.7	Pusher/Sensor Electrtonics	5+(1)	
6.0	50-meter Interferometer-control system	6+(20)	
6.1	VME Electronics	4+(16)	
6.2	Dedicated Computer	1+ (4)	
6.3	Labview Licence	1	

7.0	50-meter Interferometer-baffel study	1	
7.1	Baffles	1	
8.0	Photodesorption Study	5+(19)	
8.1	Cryostat	1+(15)	
8.2	Laser modifications & Optics	1	
8.3	RGA Cold	1+ (4)	
8.4	Cryogenics	2	
	Total Phase 1 M&S	221+(253)	118+(90)
	Phase 1 Year 1	95	28
	Phase 1 Year 2	70	60
	Phase 1 year 3	56	30

M&S Cost Estimate for P-877 Phase 2

	Element	Fermilab	CSU/JILA
		k$	k$
1.0	Upgrade two frequency locking system	10	30
1.1	Optics	10	20
1.2	Electronics		10
2.0	Upgrade Seismic Isolation System	40	
2.1	Mechanical	20	
2.2	Electronics	20	
3.0	Upgrade Interferometer	30	20
3.1	Optics	15	10
3.2	Mechanical	15	10
4.0	SSC Dipole Magnets	(1,000)	
5.0	Magnet System-Power	43	
5.1	Power bus to magnets	20	
5.2	QPM System	20	
5.3	Controls	3	
6.0	Magnet System-Cryogenics	30+(585)	
6.1	Transfer lines (45m)	5+(40)	
6.2	Transfer line expansion can	10+(65)	
6.3	Feed Can & Turn Around can	(450)	
6.4	U tubes	5+(30)	
6.5	Quench Header	5	
6.6	Instrumentation	5	
7.0	Vacuum System Upgrade	100	
7.1	Vacuum Pumps (optics Tower, beam pipe)	30	
7.2	Getter Insert	25	
7.3	Oil free turbo cart	45	
	Total Phase 2 M&S	253+(1,585)	50
	Phase 2 Year 1	190	30
	Phase 2 Year 2	63	20